(1)

University of Colorado at Boulder

DEPARTMENT OF
MECHANICAL ENGINEERING

Three Dimensional Amplification of Seismic Waves by Alluvial Valleys of Arbitrary Shape: Part I. Incident P and SV Waves

K. R. Khair
S. K. Datta
University of Colorado

A. H. Shah
University of Manitoba

CUMER-88-2 July, 1988

DTIC
ELECTE
NOV 1 6 1988
D

ACKNOWLEDGMENT

The work reported here was supported in part by a grant from the National Science Foundation (# ECE-8518604) and a grant from the Office of Naval Research (# N00014-86-K- 0280). Partial support was also received from the Natural Science and Engineering Research Council of Canada (# A-7988). One of the authors (SKD) gratefully acknowledges the support from the University of Colorado in the form of a faculty fellowship for the academic year 1986-87 during which part of this work was done.

THREE DIMENSIONAL AMPLIFICATION OF SEISMIC WAVES BY ALLUVIAL VALLEYS OF ARBITRARY SHAPE:

PART I. INCIDENT P AND SV WAVES

by

K. R. Khair

S. K. Datta

Department of Mechanical Engineering and CIRES
University of Colorado, Boulder, CO 80309–0427

and

A. H. Shah

Department of Civil Engineering, University of Manitoba
Winnipeg, CANADA R3T 2N2

ABSTRACT

Amplification of ground motion in three dimensions due to arbitrarily shaped cylindrical alluvial valleys has been investigated in this paper. A hybrid numerical method combining integral representation and finite element discretization has been employed. The incident wave is either a plane P or SV wave, propagating at an arbitrary angle to the axis of the cylindrical valley. Numerical results showing significant dynamic amplification are presented for various angles of incidence and two different geometries of the valleys.

INTRODUCTION

One of the basic problems in engineering seismology is the influence of local geological irregularities on the ground motion caused by propagating seismic waves. Analysis of many earthquakes (e.g. Mexico City earthquake 1985,San Fernando earthquake 1971) show that large amplification of ground motion occurs at topographic changes and when the material properties are softer near the surface than that of the surrounding medium. Experimental studies by Kagami et al.(1982,1985), King and Tucker(1984),and Tucker and King(1984) have confirmed this amplification phenomenon. Analytical solutions to this problem have been obtained only for simple geometries (e.g. Trifunac 1973, Wong and Trifunac 1974a, Sanchez–Sesma and Rosenblueth 1979). Analysis of more complicated geometries requires numerical techniques such as finite difference and finite elements. Large geometrical dimensions of geotechnical problems limit the applicability of these methods usually to some simple situations in two dimensoins.

To avoid the difficulties associated with the discretization of the entire domain the boundary integral equation method has been found to be effective (Sanchez–Sesma and Rosenblueth, 1979; Dravinski ,1982a,b,c; Wong, 1982; Dravinski, 1983; Dravinski and Mossessian, 1987a) for studying geotechnical problems. In this method only the boundary of the scatterer is being discretized. The main advantage is in the reduction of the number of unknown variables. However, this method can be usefully applied only when the material inside the boundary is isotropic and homogeneous (Kobayashi, 1983).

In this paper, we present a hybrid method which combines the advantages of the finite element technique and the boundary integral method. In the past it has been applied to study scattering of elastic waves in two dimensions (Franssens and Lagasse 1984 and Shah et al., 1982).

Here, we study the scattering of elastic waves due to cylindrical alluvial valleys when the plane of propagation has an arbitrary angle with the axis of the scatterer. Thus the problem is three dimensional and to our knowledge this has not been investigated before.

Numerical results are presented for semi–circular and semi–elliptical cylinderical alluvial valleys. The incident plane P and SV waves propagating at arbitrary angles are considered. Results for the particular case when the direction of incidence lies in a plane perpendicular to the axis of the cylindrical valley have been found to agree with previously published results. It is shown that amplification can be larger for directions of propagation oblique to the axis than when they are perpendicular.

STATEMENT OF THE PROBLEM

Figure 1 shows the geometry of the problem. As shown cylindrical inclusion of arbitrary surface shape with axis parallel to the y–axis (not shown) is perfectly bonded to homogeneous, isotropic elastic half–space. Let us consider two artificial boundaries C and B. The medium is, now, divided into two regions. The interior region R_1 is bounded by the boundary B and part of the free surface. The exterior region R_o is bounded by the free surface and the contour C and extends to infinity in the x and z directions. The area between the contours C and B is shared by both regions. All the inhomogeneities are assumed to lie wthin C.

We consider plane harmonic P or SV wave incident at an arbitrary angle to the y–axis (see Fig. 2). Thus the displacement has all three components.

Let u_i be the displacement component in the i–th direction in a Cartesian frame and let T_{ij} be the second order Cauchy stress tensor (i,j = 1,2,3) having time harmonic behavior of the form $e^{-i\omega t}$ where, ω, is the circular frequency (rad/sec). In each region u_i and T_{ij} satisfy the equation of motion given by Eq. (1),

$$T_{ij,j} + \rho\omega^2 u_i = -f_i, \qquad (i,j = 1,2,3) \tag{1}$$

where ρ is the mass density, f_i is the force per unit volume, and the factor, $e^{-i\omega t}$, has been dropped. The stress free boundary conditions along the surface of the half-space are specified by,

$$\sigma_{zz} = 0$$

$$\sigma_{zx} = 0$$

$$\sigma_{zy} = 0.$$

The scattered field also satisfies the radiation condition at infinity.

(I) The Exterior Region R_o

In this region the displacement u_i is composed of two parts,

$$u_i = u_i^{(o)} + u_i^{(s)}, \tag{2}$$

where $u_i^{(o)}$ is the free–field displacement (including the incident waves and their reflections from the free surface) and $u_i^{(s)}$ is the contribution of the scattered waves. The scattered displacement field is represented by a surface integral as discussed below.

Starting with Betti's reciprocity theorem (Aki& Richards 1980), a pair of solutions to Eq.(1) for the displacements can be written as

$$\int\int_A (\underline{f} \cdot \underline{v} - \underline{g} \cdot \underline{u}) = \oint_C (\underline{u} \cdot \underline{s} - \underline{v} \cdot \underline{t}) dc. \tag{3}$$

where use has been made of the radiation condition. In the above $\underline{u}$, $\underline{t}$ represent the displacement and surface traction caused by body forces $\underline{f}$, while $\underline{v}$, $\underline{s}$ are the displacement and the surface traction due to body forces $\underline{g}$ in region R_o. The scattered field is taken to be the first field. The second field is the Green's solution. The scattered field has no sources in R_o, hence $\underline{f} = 0$. For the Green's displacement field the source is represented by

$$\underline{g} = \delta(\underline{r} - \underline{r'}) e^{-i\omega t + i\xi k_2 y} \underline{e}_i,$$

where $|(r - r')| = \sqrt{(x - x')^2 + (z - z')^2}$, $\underline{e}_i$ is the unit vector in the i–th direction, and $k_2 = \omega/c_2, c_2$ being the shear wave speed in R_o. This represents a line source at (x', z')

varying in the y–direction with wavelength $\frac{2\pi}{\xi k_2}$. The expression for the Green's displacement tensor, G_{ij}, and the corresponding stresses, Σ_{ijk}, are presented in Appendix A. Substituting the expression for $\underline{g}$ into Eq.(3) and using the divergence theorm ,yields, dropping the factor $e^{i\xi k_2 y}$,

$$u_i^{(s)}(x', z') = \oint_C (G_{ij} T_{jk}^{(s)} - u_j^{(s)} \Sigma_{ijk}) n_k dc. \tag{4}$$

In writing Eq.(4) the condition of vanishing traction on the free surface z=0 and the radiation condition at infinity satisfied by the scattered and the Green's displacement fields have been utilized. The contour integration is carried out in clockwise direction and n_k are the components of the outward unit normal vector to C. Here we choose the source points (x', z') to be on the contour B inside R_o (Figure 1). This precludes the singularities arising from evaluating the integral with the source and the observer at the same location.

Now we apply Eq. (3) to the part of region R_1, which includes the scatterer and bounded by contour C. The two fields are the Green's field, with its source outside this region, and the incident field. The incident field has no sources here. This yields

$$0 = \oint_C (G_{ij} T_{jk}^{(o)} - u_j^{(o)} \Sigma_{ijk}) \ (-n_k) \ dc. \tag{5}$$

The integration along C is calculated in counterclockwise direction. $u_j^{(o)}$ and $T_{jk}^{(o)}$ denote the displacement and stress tensor associated with the incident field, respectively. Reversing the direction of integration of Eq. (5) and adding it to Eq. (4), using Eq. (2), yields

$$u_i(x', z') = \oint_C (G_{ij} T_{jk} - u_j \Sigma_{ijk}) n_k dc + u_i^{(o)}, \tag{6}$$

Eq. (6) is the integral representation of the total field at any point in the exterior region R_o.

(II) The Interior Region R_1

This region encloses all the inhomogeneities and anisotropies. In order to get the solution in region R_1 , we use the finite element technique. In this approach, the area of interest R_1 is divided into a number of elements. In each element the particle displacement is given by

$$u_i = \{\Phi_l\}^T \{u_{i;l}\} \tag{7}$$

where

$i = 1\ ,\ 2, 3$

$l = 1,\ldots..\ \mathrm{n}$ n is the number of nodes per element,

and $\{\Phi_l\}$ is an n×1 column vector representing the shape functions for the element,

$$\{\Phi_l\} = [\Phi_1 \quad \Phi_2 \cdots \Phi_n]^T \tag{8}$$

In Eq.(7) $\{u_{i;l}\}$ is the particle displacement vector corresponding to the nodal points of each element, T, $\{\cdot\}, [\cdot]$ denote a transpose, a column vector, and a row vector, respectively. The strain within an element related to the displacement field $\{u\}_e$ is given by

$$\{\epsilon\}_e = [L][\Phi]\{u\}_e, \tag{9}$$

$$= [B]\{u\}_e, \tag{10}$$

where [L] is an operator matrix

$$[L] = \begin{bmatrix} \frac{\partial}{\partial x} & 0 & 0 \\ 0 & i\xi & 0 \\ 0 & 0 & \frac{\partial}{\partial z} \\ 0 & \frac{\partial}{\partial z} & i\xi \\ \frac{\partial}{\partial z} & 0 & \frac{\partial}{\partial x} \\ i\xi & \frac{\partial}{\partial x} & 0 \end{bmatrix} \tag{11}$$

and

$$[B] = [L][\Phi] \tag{12}$$

In order to determine the elemental impedance matrix, let us consider the energy functional E,

$$\mathbf{E} = 1/2 \int\int\int (\mathbf{T}.\epsilon^* - \rho\omega^2 \mathbf{u}.\mathbf{u}^*) dxdydz - 1/2 \int\int (\mathbf{t}_B.\mathbf{u}_B^* + \mathbf{t}_B^*.\mathbf{u}_B) ds, \tag{13}$$

where $\mathbf{T}$ and ϵ are stresse and strain column vectors, respectively, defined as

$$\mathbf{T} = \{T\} = [T_{xx} T_{yy} T_{zz} T_{zy} T_{zx} T_{xy}]^T$$

and

$$\epsilon = \{\epsilon\} = [\epsilon_{xx} \epsilon_{yy} \epsilon_{zz} \epsilon_{zy} \epsilon_{zx} \epsilon_{xy}]^T$$

$\mathbf{t}_B, \mathbf{u}_B$ represent, respectively, the traction force and the displacement at the boundary B. For the purpose of eliminating the intergration over the y–direction, it can be shown that if one takes the integration over one wavelength λ, Eq.(13) becomes

$$\mathbf{E}/\lambda = 1/2 \int\int (\mathbf{T}.\epsilon^* - \rho\omega^2 \mathbf{u}.\mathbf{u}^*) dxdz - 1/2 \int (\mathbf{t}_B.\mathbf{u}_B^* + \mathbf{t}_B^*.\mathbf{u}_B) dc \tag{14}.$$

The stresses $\mathbf{T}$ are related to the strains ϵ by the constitutive equation

$$\{T\} = [D]\{\epsilon\}. \tag{15}$$

Using Eq.(15) and Eq.(7) in Eq.(14) and taking the variation, the equation of motion for region R_1 can be written as

$$\begin{bmatrix} S_{II} & S_{IB} \\ S_{BI} & S_{BB} \end{bmatrix} \begin{Bmatrix} u_I \\ u_B \end{Bmatrix} = \begin{Bmatrix} Y_I \\ Y_B \end{Bmatrix} \tag{16}$$

where the elemental impedence matrices S_{IJ} are represented by

$$[S]_e = \int\int_{Ae} ([B^*]_e^T[D][B]_e - \rho\omega^2[\Phi_e]^T[\Phi_e])dxdz \tag{17}$$

and the nodal force vector due to applied surface traction,

$$\{Y\}_e = \int_{C_e} [B^*]_e^T[D][\Phi_e]\{n\}dc. \tag{18}$$

Here A_e and C_e denotes, respectively, the area and the boundary of an element and $\{n\}$ is the unit vector normal to C_e. [D] is 6 × 6 matrix of the element material elastic constants. It is clear from Eq.(17) that $[S]_e$ is hermitian matrix. In Eq.(16) $\{u_I\}$ and $\{u_B\}$ represent the interior and boundary nodal displacements, respectively. $\{Y_B\}$ represent the interaction forces between regions R_o and R_1 at the boundary nodes. Since there are no forces on the interior nodes, hence $\{Y_I\} = 0$, and Eq.(16) becomes,

$$\begin{bmatrix} S_{II} & S_{IB} \\ S_{BI} & S_{BB} \end{bmatrix} \begin{Bmatrix} u_I \\ u_B \end{Bmatrix} = \begin{Bmatrix} 0 \\ Y_B \end{Bmatrix} \tag{19}$$

Thus by using the upper part of Eq.(19), the boundary nodal displacement $\{u_B\}$ can be related to the interior nodal displacement $\{u_I\}$ as

$$\{u_I\} = -[S_{II}]^{-1}[S_{IB}]\{u_B\}. \tag{20}$$

Now , Eq.(6) and Eq.(19) should be combined in order to solve for the displacement at the boundary nodes N_B. To achieve this Eq.(6) should be evaluated at the nodes on the boundary B.

Using the constitutive relation to express T_{ij} and Eq.(7) to present the displacement, Eq.(6) becomes

$$u(x',z') = u^{(o)}(x',z') + \left[\oint_C ([G][D][B_I] - [\Phi_I]^T[\Sigma])\{n\}dc\right]\{u_I\} + \left[\oint_C ([G][D][B_B] - [\Phi_B]^T[\Sigma])\{n\}dc\right]\{u_B\}, \tag{21}$$

where $[B_I] = [L][\Phi_I]$ and $[B_B] = [L][\Phi_B]$. Evaluating the integrals at all the nodes N_B on the boundary B, Eq.(21) can be written as

$$\{u_B\} = [A_{BI}]\{u_I\} + [A_{BB}]\{u_B\} + \{u_B^{(o)}\}, \tag{22}$$

where $[A_{BI}]$ is $3N_B$ x $3N_I$ and $[A_{BB}]$ is $3N_B \times 3N_B$ complex matrices. Substituting Eq. (20) into Eq. (22), and collecting terms, yields

$$\{u_B\} = -[A_{BI}][S_{II}]^{-1}[S_{IB}]\{u_B\} + [A_{BB}]\{u_B\} + \{u_B^{(o)}\} \tag{23}$$

Once $\{u_B\}$ is solved from Eq. (23) we then use Eq. (20) to find $\{u_I\}$. In the following we present numerical results for the displacement amplitudes on the surface of the valley.

Numerical Results

Normalization of Variables.

All the variables used in this paper are presented in dimensionless form. The material properties of the valley are normalized with respect to those of the half space. For that purpose we have chosen the shear velocity β_o and the shear modulus μ_o to be unity, distances are normalized with respect to half the width of the finite element region H, and the displacements are normalized to the absolute amplitude of the displacement of the free-field motion ($\sqrt{|u_x^{(o)}|^2 + |u_y^{(o)}|^2 + |u_z^{(o)}|^2}$). The normalized frequency ϵ is defined as

$$\epsilon = k_2 H$$

where k_2 is the shear wave number in the half space. The poisson's ratio for all the materials is taken to be 1/3.

Testing the method

Suffeciently general computer code has been written to investigate the three dimensional problem. In order to gauge the accuracy of the results we, first, let the

material of the alluvial valley to have the same properties of the half space. The calculated displacements should be equal to the free field displacements. Deviation from the free field response is taken as a test of the inaccuracy. When the error was found to be unacceptable we increased the number of elements in the interior region R_1. It was found that 6 elements per wavelength are suffecient to achieve the required accuracy.

Second, the generality of the program was tested by running the problem of scattering of plane harmonic P and SV waves by semi-circular alluvial valley when $\xi = 0$. This is a plane strain problem and was studied by Dravinski and Mossessian (1987a) for weakly inelastic materials. Figures 3 and 4 show very good agreement of the results for all the angles of incidence and both types of incident waves (P and SV) and $\epsilon = \pi$.

Semi – circular alluvial valley.

For semi-circular valley the finite element part is compsed of 190 elements. Isoparametric elements of 3 and 4 nodes are used. The number of boundary nodes N_B is 29. The number of the interior nodes N_I is 178. The depth of the finite element region in the z-direction is taken to be equal to H. The results presented here are for $\epsilon = \pi$. The area between contours B and C is occupied by one layer of elements. The shear modulus of the valley μ_1 is taken to be 1/6 and the shear velocity β_1 is 1/2. Figures 5 and 7 show the normalized amplitudes of u_x, u_y, and u_z when P and SV waves are incident in a plane making an angle 45 degree with the axis of the valley. Figures 6 and 8 show the corresponding results when the plane of propagation is parallel to the yz plane. Figure 5 shows large amplification in the y-component of the ground motion when P wave propagates with $\theta_1 = 60°$. Also, figure 7 shows large amplification when the angle of incidence of SV wave, θ_2, is 30 degree. From figures 5 and 7 it is seen that u_y is generally amplified the most compared with u_x and u_z. Comparison of Fig. 5-8 shows that, exept when SV wave is incident in the plane of yz, u_y is generally amplified

more. For SV wave incident in the yz-plane one finds large amplification in vertical displacement when $\theta_2 = 60°$. Also of interest is to note that larger amplification occur for incidence in the 45° plane.

Semi – elliptical alluvial valley

In this case different finite element mesh is used. The total number of elements is 146 , N_B and N_I are equal to 29 and 131, respectively. The ratio of the minor axis to the major axis is 0.7 and the major axis is along the x-axis. The material of the semi-elliptical valley has the same properties as that used in the semi-circular case. ϵ is again taken to be π. Figures 9 and 10 demonstrate the results for the plane strain case while figures 11, 12, 13, and 14 show the results for different angles of incidence. It is seen that larger amplifications occur in a semi-circular valley than in a semi-elliptical one. Also, it is found that for P-waves amplification increase with θ_1, but for SV-waves they remain about the same first as θ_2 increases and then decrease. Here the most amplification of displacements occurs when P wave propagates in a plane parallel to the axis of valley and $\theta_1 = 60°$ and when SV wave propagates in that plane but with angle $\theta_2 = 30°$. In contrast with the semi-circular valley we find that u_y is amplified most for the semi-elliptical valley.

Conclusion

A hybrid numerical method hes been employed to investigate the three dimensional amplification of ground motion due to arbitrarily shaped cylindrical soft valley. This method combines the integral representation and the finite element techniques. Numerical results are presented for different angles of incidence. These results show large local amplification when the plane of propagation is oblique to or contains the axis of the valley. This finding is rather important, because so far only two-dimensional problems have been studied. It also shows significant influence of the shapes of the valley on the ground motion.

This method is also applicable to study the scattering of SH and Rayleigh waves and to a layered medium. These results will be communicated later. The very important feature of this method is that the calculations of Green's function and stresses are independent of the shape and the material of the valley. This means that for different shapes of valley and the same frequency the Green's functions and stresses has to be calculated only one time. This is the most time consuming part of the solution. This differs from an indirect boundary integral equation formulated on the boundary of the scatterer for which Green's tensor has to be recalculated at each change in the geometry of the scatterer.

REFERENCES

Dravinski, M. (1982a). Influence of interface depth upon strong ground motion, *bull. Seism. Soc. Am.* **72**, 596–614.

Dravinski, M. (1982b). Scattering of SH waves by subsurface topography, *J. Eng. Mech. Div.* **108**, 1–16.

Dravinski, M. (1982c). Scattering of elastic waves by alluvial valley, *J. Eng. Mech. Div.* **108**, 19–31.

Dravinski, M. (1983). Scattering of plane harmonic SH waves by dipping layers of arbitrary shape, *Bull. Seism. Soc. Am.* **73**, 1303–1319.

Dravinski, M. and T. K. Mossessian (1987a). Scattering of plane harmonic P, SV, and Rayleigh waves by dipping layers of arbitrary shape, *Bull. Seism. Soc. Am.* **77**, 212–235.

Kagami, H., C. M. Duke, G. C. Liang, and Y. Ohta (1982). Observation of 1– to 5– second microtremors and their application to earthquake engineering. Part II. Evaluation of site effect upon seismic wave amplification due to extremely deep soil deposits,*Bull. Seism. Soc. Am.* **72**, 987–998.

Kagami, H., S. Okada, S. Shiono, M. Oner, M. Dravinski, and A. Mal (1985). Observation of 1– to 5– second microtremors and their application to earthquake engineering. Part III. A two dimensional study of site effect in the San Fernando valley ,*Bull. Seism. Soc. Am.* **76**, 1801–1812.

King, J. L. and B. E. Tucker (1984). Observed variation of earthquake motion across a sediment– filled valley, *Bull. Seism. Soc. Am.* **74**, 137–151.

Trifunac, M. D. (1973). Scattering of plane SH wave by semicylindrical canyon, *Int. J. Earthquake Eng. and Struct. Dyn.*, bf 1, 267–281.

Tucker, B. E. and J. L. King (1984). Dependency of sediment– filled valley response on the input amplitude and the valley properties, *Bull. Seism. Soc. Am.* **74**, 153–165.

Sanchez - Sesma, F. Y. and E. Rosenblueth (1979). Ground motion at canyons of arbitrary shapes under incident SH wave, *Earthquake Eng. Struct. Dyn.*, **7**, 441–450.

Shah, A. H., K.C. Wong, and S. K. Datta (1982). Diffraction of plane SH waves in a half-space, *Earthquake Eng. Struct. Dyn.* **10**, 519–528.

Wong, H. L. (1982). Diffraction of P, SV, and Rayleigh waves by surface topographies, *Bull. Seism. Soc. Am.* **72**, 1167–1184.

Wong, H. and M. D. Trifunac (1974a). Scattering of plane SH wave by a semi-elliptical canyon, *Int. J. Earthquake Eng. Struct. Dyn.*, **3**, 157–169.

APPENDIX A

Green's Function and Stresses.

(I) Displacements

$$G_{11} = \frac{i}{2\pi\mu}\int_0^\infty g_{11}e^{i\epsilon\xi y}\cos\epsilon k(x-x')dk \qquad G_{12} = \frac{-1}{2\pi\mu}\int_0^\infty g_{12}e^{i\epsilon\xi y}\sin\epsilon k(x-x')dk$$

$$G_{13} = \frac{-1}{2\pi\mu}\int_0^\infty g_{13}e^{i\epsilon\xi y}\sin\epsilon k(x-x')dk \qquad G_{21} = \frac{-1}{2\pi\mu}\int_0^\infty g_{21}e^{i\epsilon\xi y}\sin\epsilon k(x-x')dk$$

$$G_{22} = \frac{i}{2\pi\mu}\int_0^\infty g_{22}e^{i\epsilon\xi y}\cos\epsilon k(x-x')dk \qquad G_{23} = \frac{i}{2\pi\mu}\int_0^\infty g_{23}e^{i\epsilon\xi y}\cos\epsilon k(x-x')dk$$

$$G_{31} = \frac{-1}{2\pi\mu}\int_0^\infty g_{31}e^{i\epsilon\xi y}\sin\epsilon k(x-x')dk \qquad G_{32} = \frac{i}{2\pi\mu}\int_0^\infty g_{32}e^{i\epsilon\xi y}\cos\epsilon k(x-x')dk$$

$$G_{33} = \frac{i}{2\pi\mu}\int_0^\infty g_{33}e^{i\epsilon\xi y}\cos\epsilon k(x-x')dk$$

where

$$g_{11} = \frac{k}{\gamma_1}(ke^{\pm i\gamma_1\epsilon(z-z')} - U_{1x}) + \frac{1}{1-\xi^2}(\gamma_2 e^{\pm i\gamma_2\epsilon(z-z')} + U_{2x}) + \frac{k\xi}{\gamma_2(1-\xi^2)}(k\xi e^{\pm i\gamma_2\epsilon(z-z')} - U_{3x})$$

$$g_{12} = \frac{k}{\gamma_1}(\xi e^{\pm i\gamma_1\epsilon(z-z')} - U_{1y}) + \frac{1}{1-\xi^2}U_{2y} - \frac{k\xi}{\gamma_2(1-\xi^2)}[(1-\xi^2)e^{\pm i\gamma_2\epsilon(z-z')} + U_{3y}]$$

$$g_{13} = \frac{k}{\gamma_1}(\pm\gamma_1 e^{\pm i\gamma_1\epsilon(z-z')} - U_{1z}) + \frac{1}{1-\xi^2}(\mp k e^{\pm i\gamma_2\epsilon(z-z')} + U_{2z})$$
$$- \frac{k\xi}{\gamma_2(1-\xi^2)}(\mp\gamma_2\xi e^{\pm i\gamma_2\epsilon(z-z')} + U_{3z})$$

$$g_{21} = \frac{\xi}{\gamma_1}(k e^{\pm i\gamma_1\epsilon(z-z')} - U_{1z}) + \frac{1}{\gamma_2}(-k\xi e^{\pm i\gamma_2\epsilon(z-z')} + U_{3z})$$

$$g_{22} = \frac{\xi}{\gamma_1}(\xi e^{\pm i\gamma_1\epsilon(z-z')} - U_{1y}) + \frac{1}{\gamma_2}((1-\xi^2)e^{\pm i\gamma_2\epsilon(z-z')} + U_{3y})$$

$$g_{23} = \frac{\xi}{\gamma_1}(\pm\gamma_1 e^{\pm i\gamma_1\epsilon(z-z')} - U_{1z}) + \frac{1}{\gamma_2}(\mp\gamma_2\xi e^{\pm i\gamma_2\epsilon(z-z')} + U_{3z})$$

$$g_{31} = (\pm k e^{\pm i\gamma_1\epsilon(z-z')} + U_{1z}) + \frac{k}{(1-\xi^2)\gamma_2}(\mp\gamma_2 e^{\pm i\gamma_2\epsilon(z-z')} + U_{2z})$$
$$+ \frac{\xi}{(1-\xi^2)}(\pm k\xi e^{\pm i\gamma_2\epsilon(z-z')} + U_{3z})$$

$$g_{32} = (\pm\xi e^{\pm i\gamma_1\epsilon(z-z')} + U_{1y}) + \frac{k}{(1-\xi^2)\gamma_2}U_{2y}$$
$$+ \frac{\xi}{(1-\xi^2)}[\mp(1-\xi^2)e^{\pm i\gamma_2\epsilon(z-z')} + U_{3y}]$$

$$g_{33} = (\gamma_1 e^{\pm i\gamma_1 \epsilon(z-z')} + U_{1z}) + \frac{k}{(1-\xi^2)\gamma_2}(k e^{\pm i\gamma_2 \epsilon(z-z')} + U_{2z})$$
$$+ \frac{\xi}{(1-\xi^2)}(\gamma_2 \xi e^{\pm i\gamma_2 \epsilon(z-z')} + U_{3z})$$

$$U_{1x} = \{kQe^{i\gamma_1 \epsilon z} - \frac{4k\gamma_1\gamma_2(1-2K^2)}{F} e^{i\gamma_2 \epsilon z}\} e^{i\gamma_1 \epsilon z'}$$

$$U_{2x} = \{\frac{4k^2\gamma_2(1-2K^2)}{F} e^{i\gamma_1 \epsilon z} + Pe^{i\gamma_2 \epsilon z}\} e^{i\gamma_2 \epsilon z'}$$

$$U_{3x} = \{\frac{4k\xi{\gamma_2}^2(1-2K^2)}{F} e^{i\gamma_1 \epsilon z} - (\xi kQ + \frac{8\xi k\gamma_1\gamma_2}{F}) e^{i\gamma_2 \epsilon z}\} e^{i\gamma_2 \epsilon z'}$$

$$U_{1y} = \{\xi Qe^{i\gamma_1 \epsilon z} - \frac{4\xi\gamma_1\gamma_2(1-2K^2)}{F} e^{i\gamma_2 \epsilon z}\} e^{i\gamma_1 \epsilon z'}$$

$$U_{2y} = \{\frac{4k\xi\gamma_2(1-2K^2)}{F} e^{i\gamma_1 \epsilon z} - \frac{8k\xi\gamma_1{\gamma_2}^2}{F} e^{i\gamma_2 \epsilon z}\} e^{i\gamma_2 \epsilon z'}$$

$$U_{3y} = \{\frac{4\xi^2{\gamma_2}^2(1-2K^2)}{F} e^{i\gamma_1 \epsilon z} + (1 - \xi^2 Q - \frac{8\xi^2\gamma_1\gamma_2}{F}) e^{i\gamma_2 \epsilon z}\} e^{i\gamma_2 \epsilon z'}$$

$$U_{1z} = \{\gamma_1 Qe^{i\gamma_1 \epsilon z} + \frac{4K^2\gamma_1(1-2K^2)}{F} e^{i\gamma_2 \epsilon z}\} e^{i\gamma_1 \epsilon z'}$$

$$U_{2z} = \{\frac{4k\gamma_1\gamma_2(1-2K^2)}{F} e^{i\gamma_1 \epsilon z} - kQe^{i\gamma_2 \epsilon z}\} e^{i\gamma_2 \epsilon z'}$$

$$U_{3z} = \{\frac{4\xi\gamma_1\gamma_2{}^2(1-2K^2)}{F}e^{i\gamma_1\epsilon z} - \xi\gamma_2 Q e^{i\gamma_2\epsilon z}\}e^{i\gamma_2\epsilon z'}$$

$$P = (\gamma_2 - \frac{8k^2\gamma_1\gamma_2{}^2}{F})$$

$$Q = (1 - \frac{8K^2\gamma_1\gamma_2}{F})$$

$$F = (1-2K^2)^2 + 4K^2\gamma_1\gamma_2)$$

$$\gamma_2 = \sqrt{1-K^2} \quad \gamma_1 = \sqrt{\eta^2 - K^2} \quad K = \sqrt{k^2+\xi^2}$$

$$\eta = k_1/k_2 \quad \epsilon = k_2 H$$

k_1 = Longitudinal wave number = ω/c_1.

c_1 = Longitudinal wave velocity in R_o.

Note that in the above the coordinates x,y,z have been nondimensionalized with respect to H and the $\pm$ sign correspond to z > or < z', respectively.

(II) Stresses

$$\Sigma_{1xz} = \frac{-ik_2}{2\pi}\int_0^\infty \left[(\eta^{-2}-2)\{kg_{11} + \xi g_{12} + \frac{1}{i\epsilon}\frac{\partial}{\partial z}g_{13}\} + 2kg_{11}\right] dk \sin\epsilon k(x-x')e^{i\epsilon\xi y}$$

$$\Sigma_{1yz} = -\frac{k_2}{2\pi}\int_0^\infty [\xi g_{11} + k g_{12}]\cos \epsilon k(x-x')e^{i\epsilon\xi y}dk$$

$$\Sigma_{1zz} = -\frac{k_2}{2\pi}\int_0^\infty [\frac{1}{i\epsilon}\frac{\partial}{\partial z}g_{11} + k g_{13}]\cos \epsilon k(x-x')e^{i\epsilon\xi y}dk$$

$$\Sigma_{1yz} = -i\frac{k_2}{2\pi}\int_0^\infty [\frac{1}{i\epsilon}\frac{\partial}{\partial z}g_{12} + \xi g_{13}]\sin \epsilon k(x-x')e^{i\epsilon\xi y}dk$$

$$\Sigma_{1zz} = \frac{-ik_2}{2\pi}\int_0^\infty \left[(\eta^{-2}-2)\{k g_{11} + \xi g_{12} + \frac{1}{i\epsilon}\frac{\partial}{\partial z}g_{13}\} + 2\frac{1}{i\epsilon}\frac{\partial}{\partial z}g_{13}\right]\sin \epsilon k(x-x')e^{i\epsilon\xi y}dk$$

$$\Sigma_{2zz} = \frac{-k_2}{2\pi}\int_0^\infty \left[(\eta^{-2}-2)\{k g_{21} + \xi g_{22} + \frac{1}{i\epsilon}\frac{\partial}{\partial z}g_{23}\} + 2k g_{21}\right]\cos \epsilon k(x-x')e^{i\epsilon\xi y}dk$$

$$\Sigma_{2yz} = -i\frac{k_2}{2\pi}\int_0^\infty [\xi g_{21} + k g_{22}]\sin \epsilon k(x-x')e^{i\epsilon\xi y}dk$$

$$\Sigma_{2zz} = -i\frac{k_2}{2\pi}\int_0^\infty [\frac{1}{i\epsilon}\frac{\partial}{\partial z}g_{21} + k g_{23}]\sin \epsilon k(x-x')e^{i\epsilon\xi y}dk$$

$$\Sigma_{2yz} = -\frac{k_2}{2\pi}\int_0^\infty [\frac{1}{i\epsilon}\frac{\partial}{\partial z}g_{22} + \xi g_{23}]\cos \epsilon k(x-x')e^{i\epsilon\xi y}dk$$

$$\Sigma_{2zz} = \frac{-k_2}{2\pi}\int_0^\infty \left[(\eta^{-2}-2)\{k g_{21} + \xi g_{22} + \frac{1}{i\epsilon}\frac{\partial}{\partial z}g_{23}\} + 2\frac{1}{i\epsilon}\frac{\partial}{\partial z}g_{23}\right]\cos \epsilon k(x-x')e^{i\epsilon\xi y}dk$$

$$\Sigma_{3xx} = \frac{-k_2}{2\pi} \int_0^\infty \left[(\eta^{-2} - 2)\{k g_{31} + \xi g_{32} + \frac{1}{i\epsilon} \frac{\partial}{\partial z} g_{33}\} + 2k g_{31} \right] \cos \epsilon k (x - x') e^{i\epsilon\xi y} dk$$

$$\Sigma_{3yx} = -i \frac{k_2}{2\pi} \int_0^\infty [\xi g_{31} + k g_{32}] \sin \epsilon k (x - x') e^{i\epsilon\xi y} dk$$

$$\Sigma_{3xx} = -i \frac{k_2}{2\pi} \int_0^\infty [\frac{1}{i\epsilon} \frac{\partial}{\partial z} g_{31} + k g_{33}] \sin \epsilon k (x - x') e^{i\epsilon\xi y} dk$$

$$\Sigma_{3yz} = -\frac{k_2}{2\pi} \int_0^\infty [\frac{1}{i\epsilon} \frac{\partial}{\partial z} g_{32} + \xi g_{33}] \cos \epsilon k (x - x') e^{i\epsilon\xi y} dk$$

$$\Sigma_{3zz} = \frac{-k_2}{2\pi} \int_0^\infty \left[(\eta^{-2} - 2)\{k g_{31} + \xi g_{32} + \frac{1}{i\epsilon} \frac{\partial}{\partial z} g_{33}\} + 2 \frac{1}{i\epsilon} \frac{\partial}{\partial z} g_{33} \right] \cos \epsilon k (x - x') e^{i\epsilon\xi y} dk$$

APPENDIX B

Incident Displacement

(I) Pwave

Let us consider P-wave incident in the XZ plane. The incident and reflected potentials can be written as :

$$\Phi^{(i)} = e^{i\epsilon(-\gamma_1 Z + KX - \omega t)}$$

$$\Phi^{(r)} = a_1 e^{i\epsilon(\gamma_1 Z + KX - \omega t)}$$

$$\Psi^{(r)} = b_1 e^{i\epsilon(\gamma_2 Z + KX - \omega t)}$$

The components of the displacement vector in the XZ plane, U_X, U_Z, can be derived from,

$$\mathbf{u} = \nabla\Phi + \nabla \wedge (\mathbf{e}_Y \Psi)$$

where $\Phi = \Phi^{(i)} + \Phi^{(r)}$ and $\Psi = \Psi^{(r)}$.

Displacements in the xz plane are related to those in the XZ plane by the following relations,

$$u_x = U_X cos\phi \qquad and \qquad u_y = U_X sin\phi.$$

The full expressions for u_x, u_y, u_z are documented below.

$$u_x = i\{k(a_1 e^{i\alpha_1} + e^{i\alpha_3}) - b_1\gamma_2 cos\phi\ e^{i\alpha_2}\}e^{i\epsilon(kx+\xi y)}$$

$$u_y = i\{\xi(a_1 e^{i\alpha_1} + e^{i\alpha_3}) - b_1\gamma_2 sin\phi\ e^{i\alpha_2}\}e^{i\epsilon(kx+\xi y)}$$

$$u_z = i\{\gamma_2(a_1 e^{i\alpha_1} - e^{i\alpha_3}) + b_1 K e^{i\alpha_2}\}e^{i\epsilon(kx+\xi y)}$$

$$a_1 = \frac{(1-2K^2)^2 - 4K^2\gamma_1\gamma_2}{F}, \qquad b_1 = \frac{-4K\gamma_1(1-K^2)}{F}$$

$$F = (1 - 2K^2)^2 + 4K^2\gamma_1\gamma_2$$

$$\alpha_1 = \epsilon\gamma_1 z\,, \quad \alpha_2 = \epsilon\gamma_2 z\,, \quad \alpha_3 = -\epsilon\gamma_1 z$$

$$k = \eta\ sin\theta_1\ cos\phi\,, \quad \xi = \eta\ sin\theta_1\ sin\phi\,, \quad K^2 = \xi^2 + k^2$$

θ_1 = angle of incidence with the negative Z-axis in the XZ plane ($0^o \leq \theta_1 \leq 90^o$).

ϕ = angle between xz plane and XZ plane ($0^o \leq \phi \leq 180^o$).

(II) SVwave

Let us consider incident SV–wave in the XZ plane:

$$\Psi^{(i)} = e^{i\epsilon(-\gamma_2 Z + KX - \omega t)}$$

$$\Phi^{(r)} = a_2 e^{i\epsilon(\gamma_1 Z + KX - \omega t)}$$

$$\Psi^{(r)} = b_2 e^{i\epsilon(\gamma_2 Z + KX - \omega t)}$$

Following the same steps as before in the P-wave, we get:

$$a_2 = \frac{-4K\gamma_2(1 - K^2)}{F}$$

$$b_2 = -\frac{(1-2K^{-2})^2 - 4K^{-2}\gamma_1\gamma_2}{F}$$

$$u_x = i\{ka_2 e^{i\alpha_1} + \gamma_2 cos\phi[e^{i\alpha_3} - b_2 e^{i\alpha_2}]\}e^{i\epsilon(kx+\xi y)}$$

$$u_y = i\{\xi a_2 e^{i\alpha_1} + \gamma_2 sin\phi[e^{i\alpha_3} - b_2 e^{i\alpha_2}]\}e^{i\epsilon(kx+\xi y)}$$

$$u_z = i\{\gamma_1 a_2 e^{i\alpha_1} + K[e^{i\alpha_3} + b_2 e^{i\alpha_2}]\}e^{i\epsilon(kx+\xi y)}$$

where $\alpha_3 = -\epsilon\ \gamma_2\ z\,,$ $k = sin\theta_2\ cos\phi\,,$ $\xi = sin\theta_2\ sin\phi$

and θ_2 is the incidence angle with the negative Z-axis in the XZ plane.

List of Figures

Fig.9 : Normalized Surface Displacement Amplitude for Semi-Elliptical Alluvial Valley.

($\epsilon = \pi, \mu_o = 1, \nu_o = 1/3, \beta_o = 1.0$

$\mu_1 = 1/6, \nu_1 = 1/3, \beta_1 = 0.5$, Minor Axis/Major Axis = 0.7)

(a) Incident P-wave: $\phi = 0^o$, $\theta_1 = 0^o$.

(b) Incident P-wave: $\phi = 0^o$, $\theta_1 = 30^o$.

(c) Incident P-wave: $\phi = 0^o$, $\theta_1 = 60^o$.

Fig.10 : Normalized Surface Displacement Amplitude for Semi-Elliptical Alluvial Valley.

(a) Incident SV-wave: $\phi = 0^o$, $\theta_2 = 0^o$.

(b) Incident SV-wave: $\phi = 0^o$, $\theta_2 = 30^o$.

(c) Incident SV-wave: $\phi = 0^o$, $\theta_2 = 60^o$.

Fig.11 : Normalized Surface Displacement Amplitude for Semi-Elliptical Alluvial Valley.

(a) Incident P-wave: $\phi = 45^o$, $\theta_1 = 30^o$.

(b) Incident P-wave: $\phi = 45^o$, $\theta_1 = 60^o$.

Fig.12 : Normalized Surface Displacement Amplitude for Semi-Elliptical Alluvial Valley.

(a) Incident P-wave: $\phi = 90^o$, $\theta_1 = 30^o$.

(b) Incident P-wave: $\phi = 90^o$, $\theta_1 = 60^o$.

Fig.13 : Normalized Surface Displacement Amplitude for Semi-Elliptical Alluvial Valley.

(a) Incident SV-wave: $\phi = 45^o$, $\theta_2 = 30^o$.

(b) Incident SV-wave: $\phi = 45^o$, $\theta_2 = 60^o$.

Fig.14 : Normalized Surface Displacement Amplitude for Semi-Elliptical Alluvial Valley.

(a) Incident SV-wave: $\phi = 90^o$, $\theta_2 = 30^o$.

(b) Incident SV-wave: $\phi = 90^o$, $\theta_2 = 60^o$.

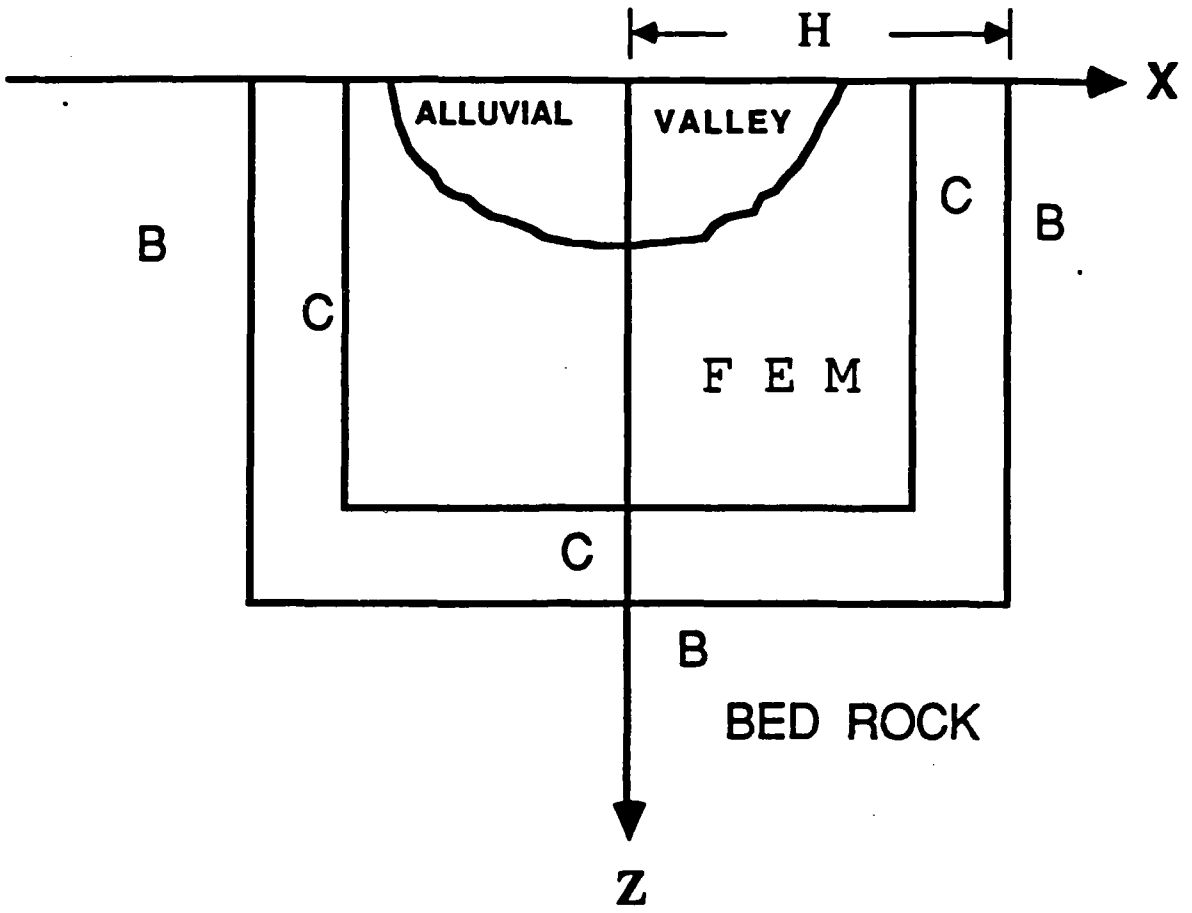

Fig. 1 Geometry of the problem

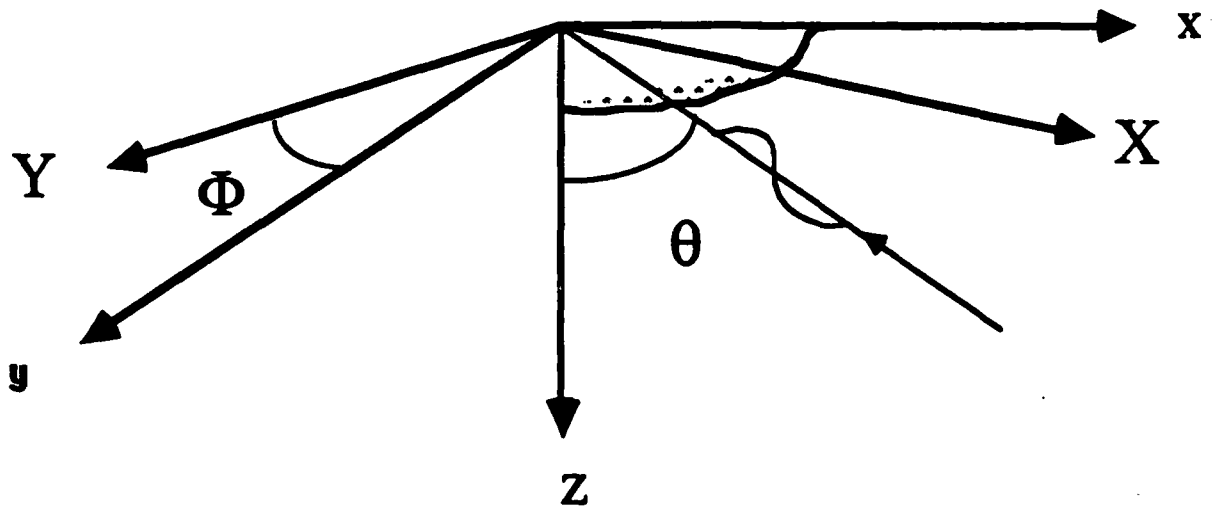

Fig. 2 The arrow indicates the incident plane wave direction which lies in the plane of Xz that makes an angle ϕ with the plane of xz

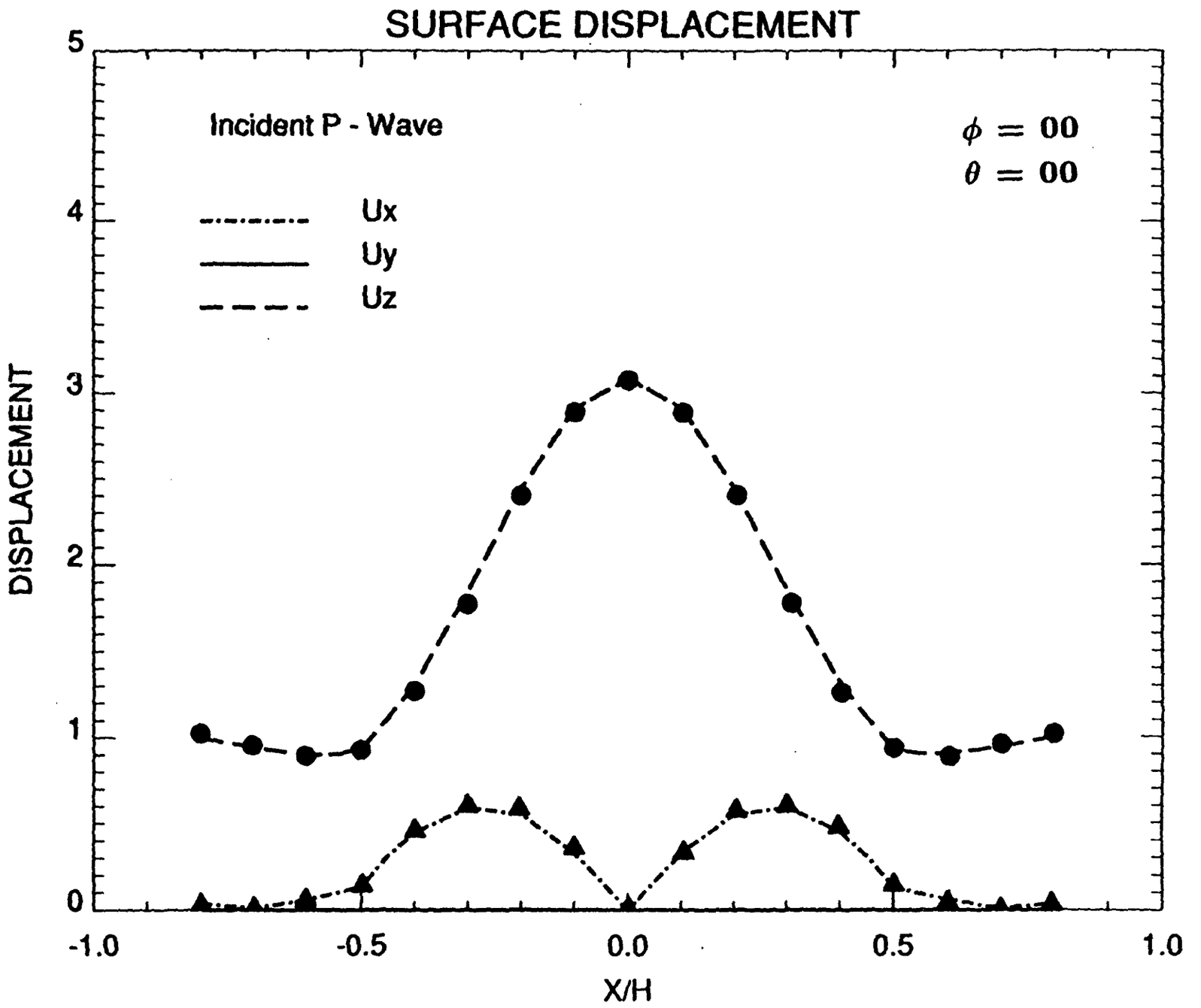
SURFACE DISPLACEMENT
Incident P - Wave
$\phi = 00$
$\theta = 00$
Ux
Uy
Uz
DISPLACEMENT
X/H
5
4
3
2
1
0
-1.0
-0.5
0.0
0.5
1.0

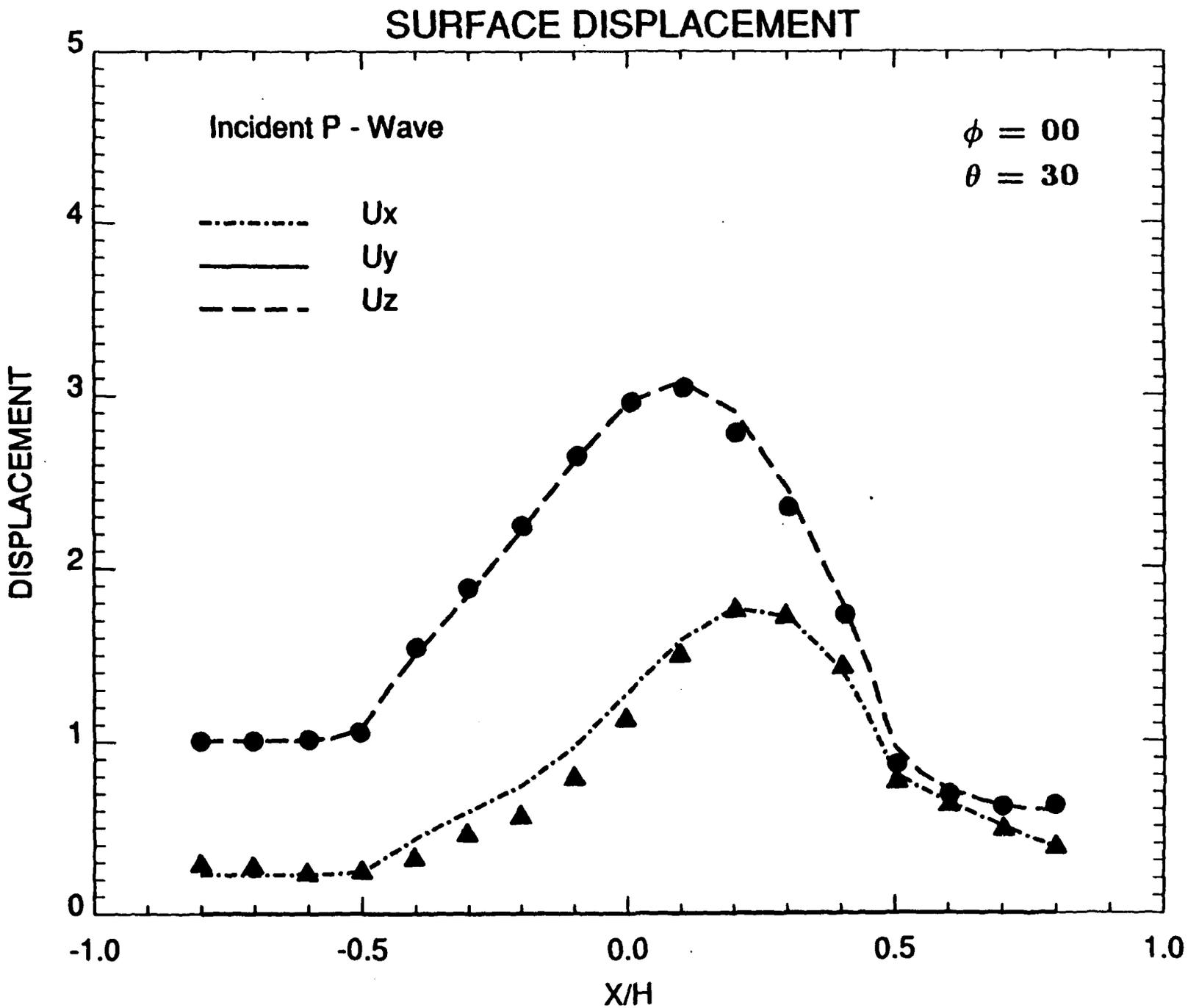
SURFACE DISPLACEMENT
Incident P - Wave
$\phi = 00$
$\theta = 30$
Ux
Uy
Uz
DISPLACEMENT
X/H
5
4
3
2
1
0
-1.0
-0.5
0.0
0.5
1.0

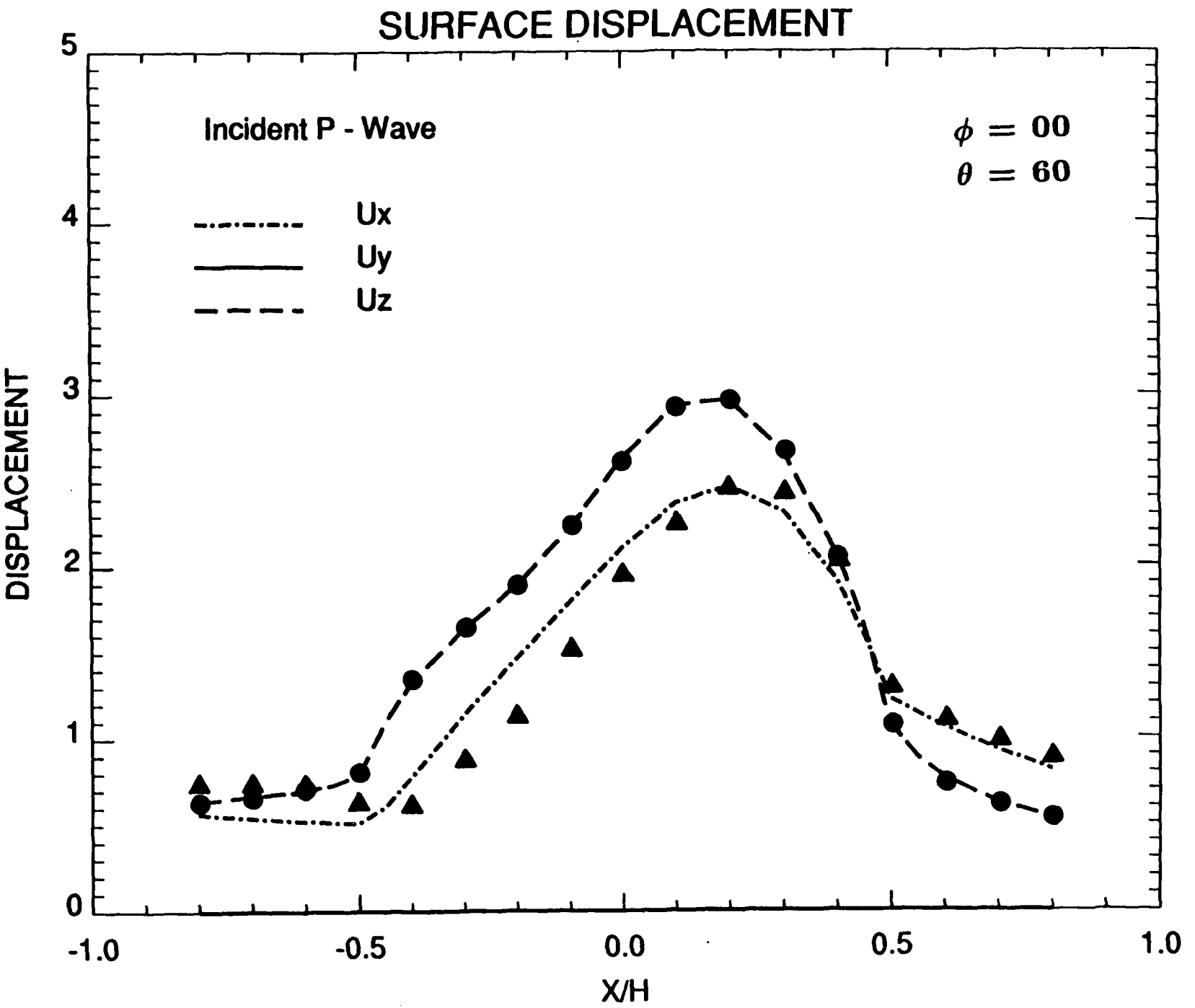
SURFACE DISPLACEMENT
Incident P - Wave
$\phi = 00$
$\theta = 60$
Ux
Uy
Uz
DISPLACEMENT
X/H
5
4
3
2
1
0
-1.0
-0.5
0.0
0.5
1.0

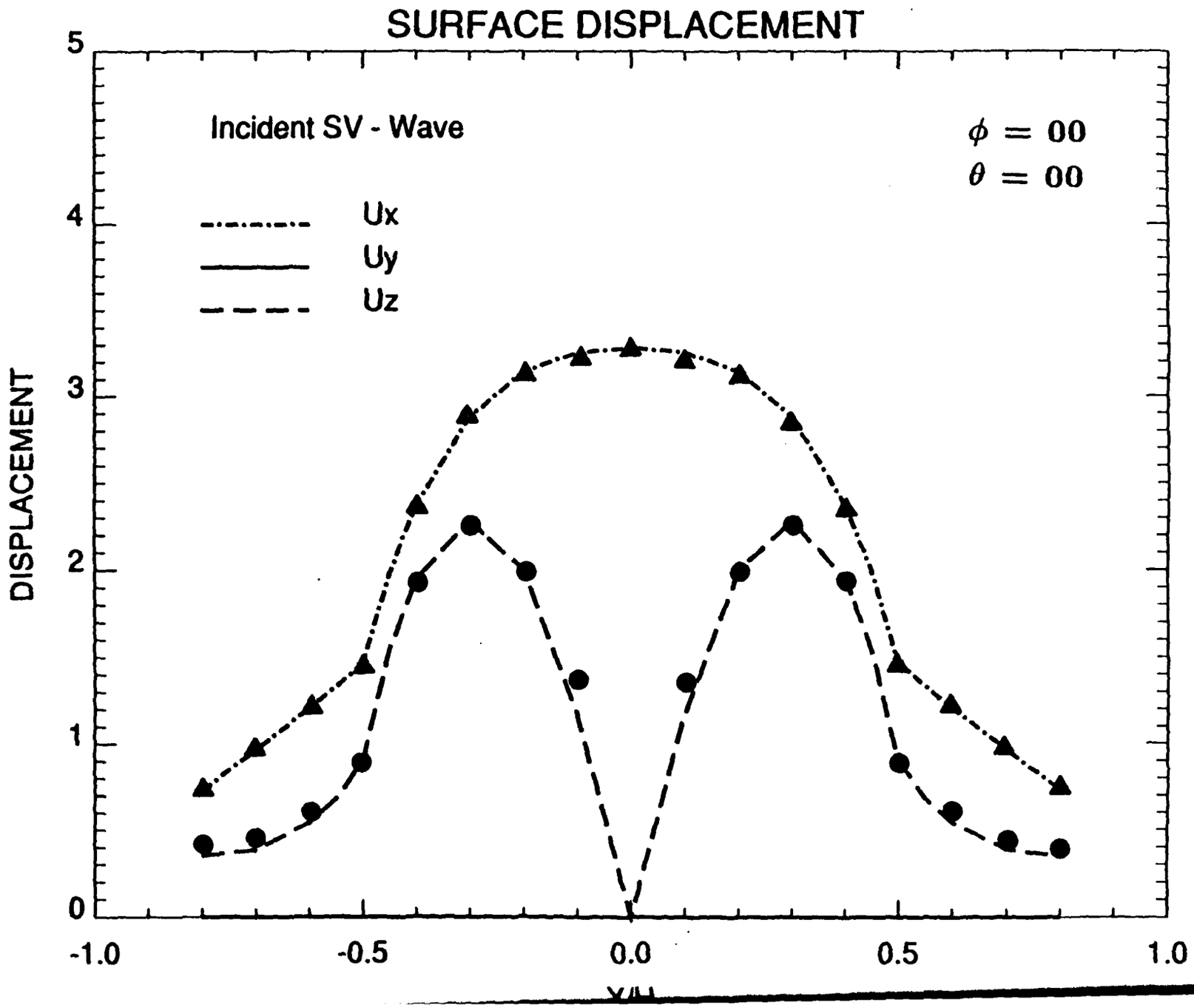
SURFACE DISPLACEMENT
Incident SV - Wave
$\phi = 00$
$\theta = 00$
Ux
Uy
Uz
DISPLACEMENT
5
4
3
2
1
0
-1.0
-0.5
0.0
0.5
1.0

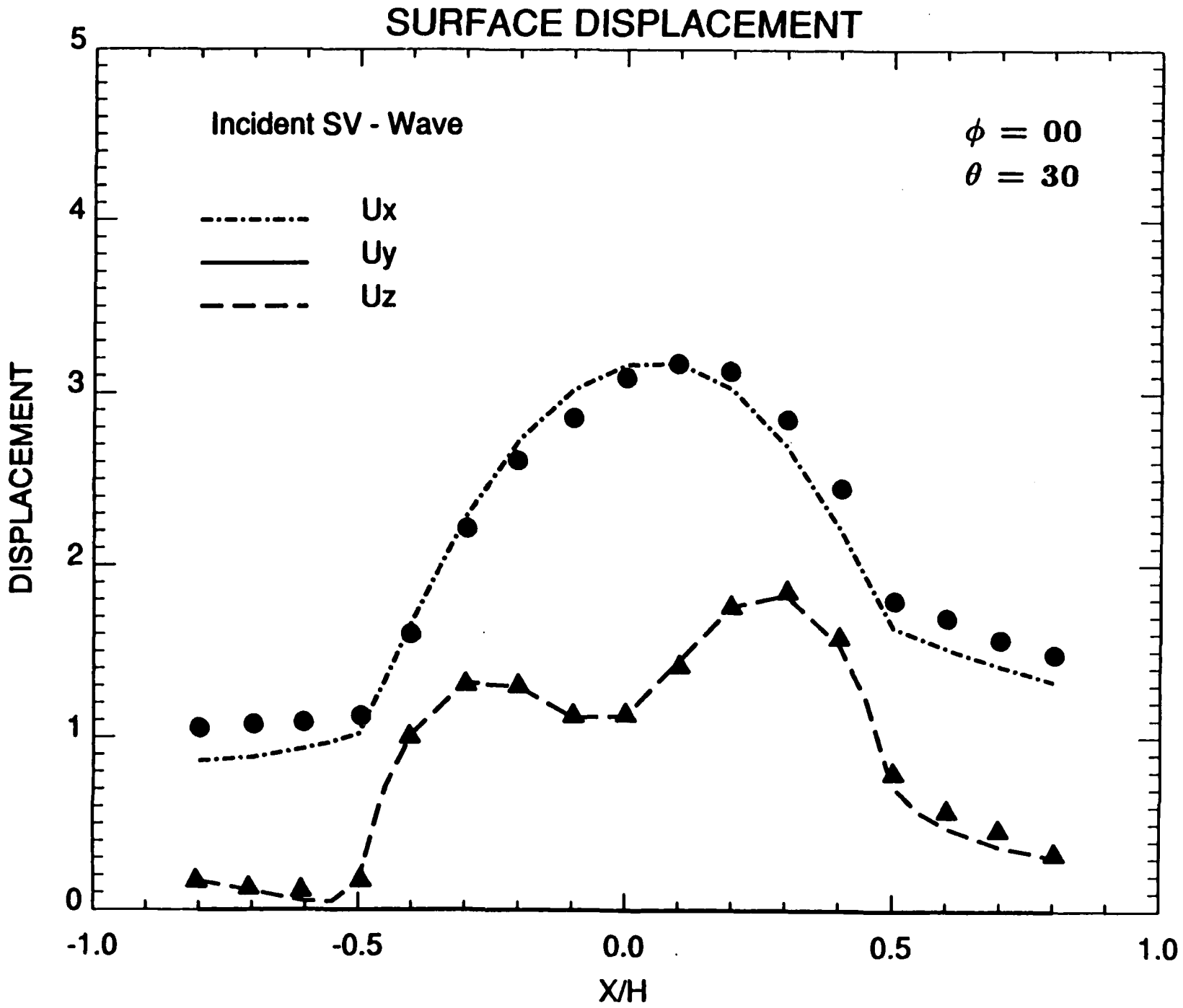
SURFACE DISPLACEMENT
Incident SV - Wave
$\phi = 00$
$\theta = 30$
Ux
Uy
Uz
DISPLACEMENT
5
4
3
2
1
0
-1.0
-0.5
0.0
0.5
1.0
X/H

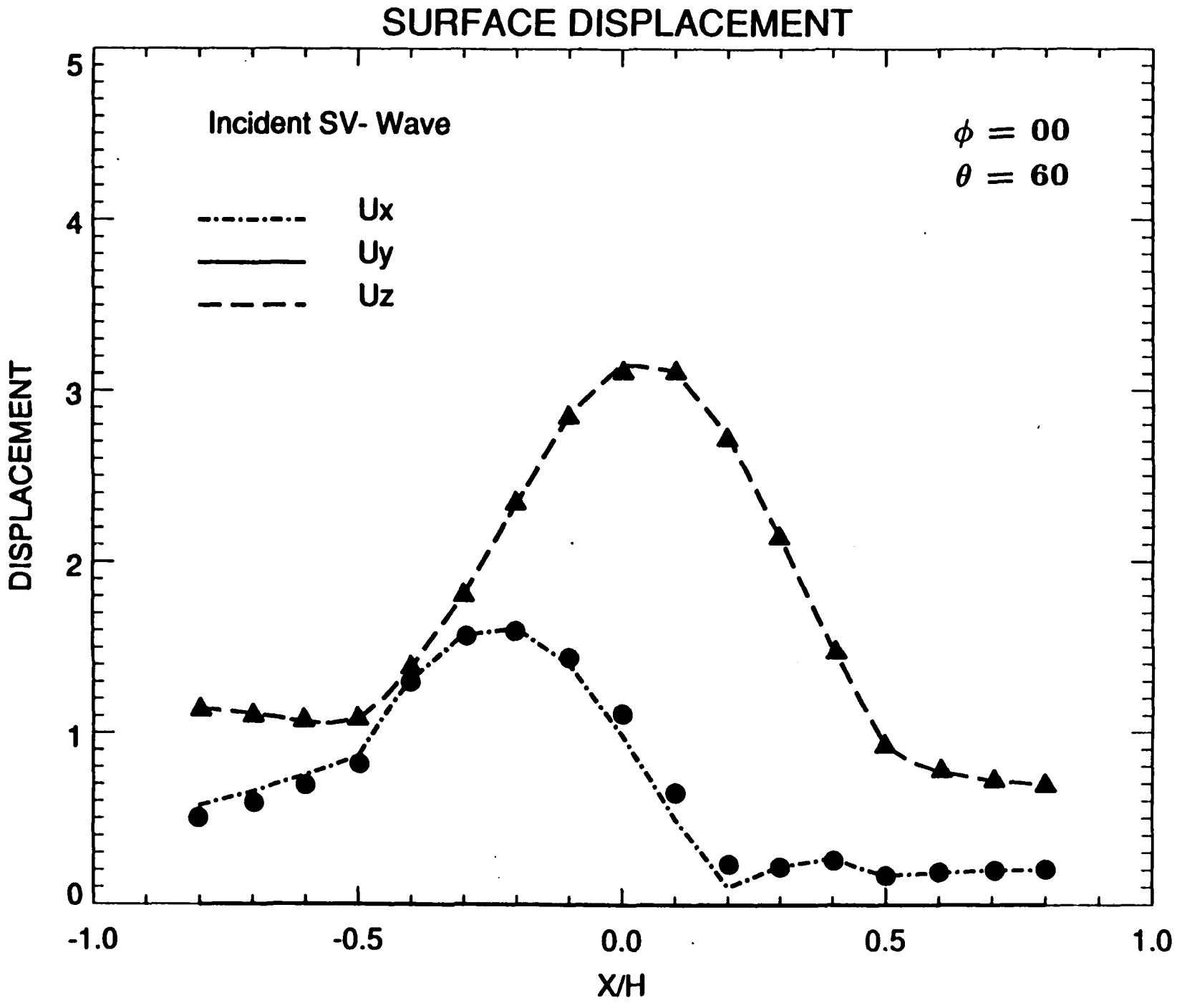
SURFACE DISPLACEMENT
Incident SV- Wave
$\phi = 00$
$\theta = 60$
Ux
Uy
Uz
DISPLACEMENT
X/H
5
4
3
2
1
0
-1.0
-0.5
0.0
0.5
1.0

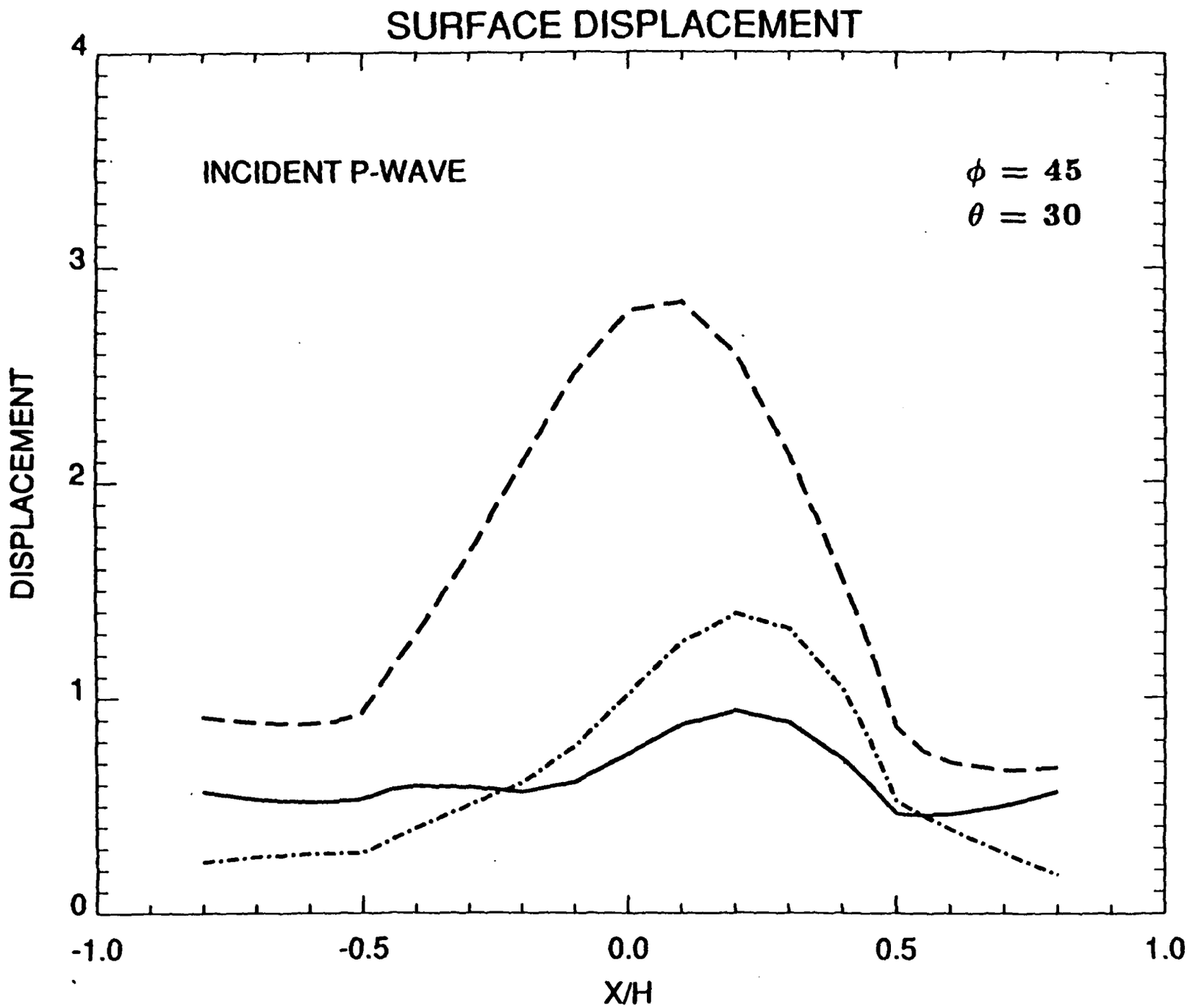
SURFACE DISPLACEMENT
INCIDENT P-WAVE
$\phi = 45$
$\theta = 30$
DISPLACEMENT
4
3
2
1
0
-1.0
-0.5
0.0
0.5
1.0
X/H

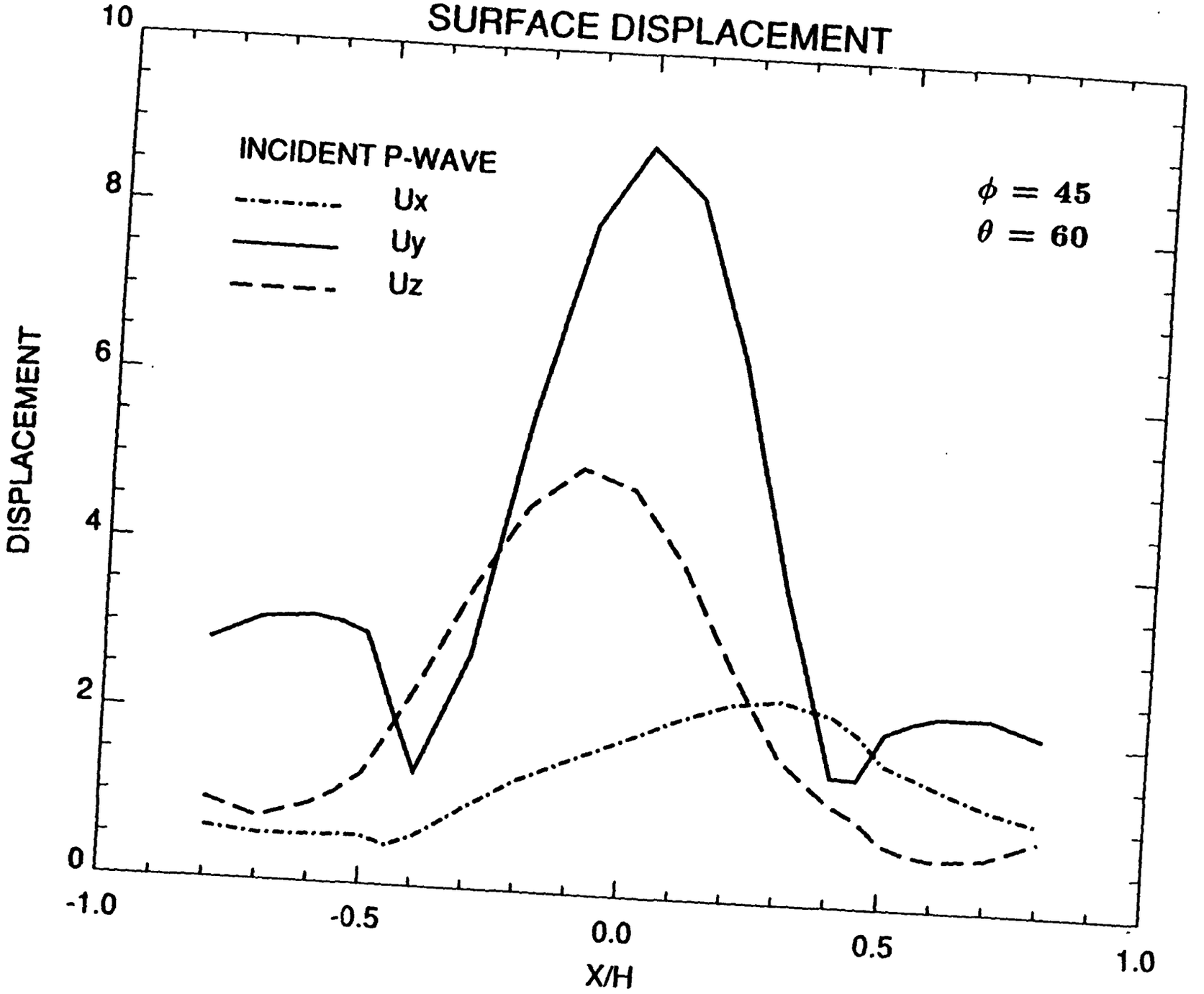
SURFACE DISPLACEMENT
INCIDENT P-WAVE
Ux
Uy
Uz
$\phi = 45$
$\theta = 60$
DISPLACEMENT
10
8
6
4
2
0
-1.0
-0.5
0.0
0.5
1.0
X/H

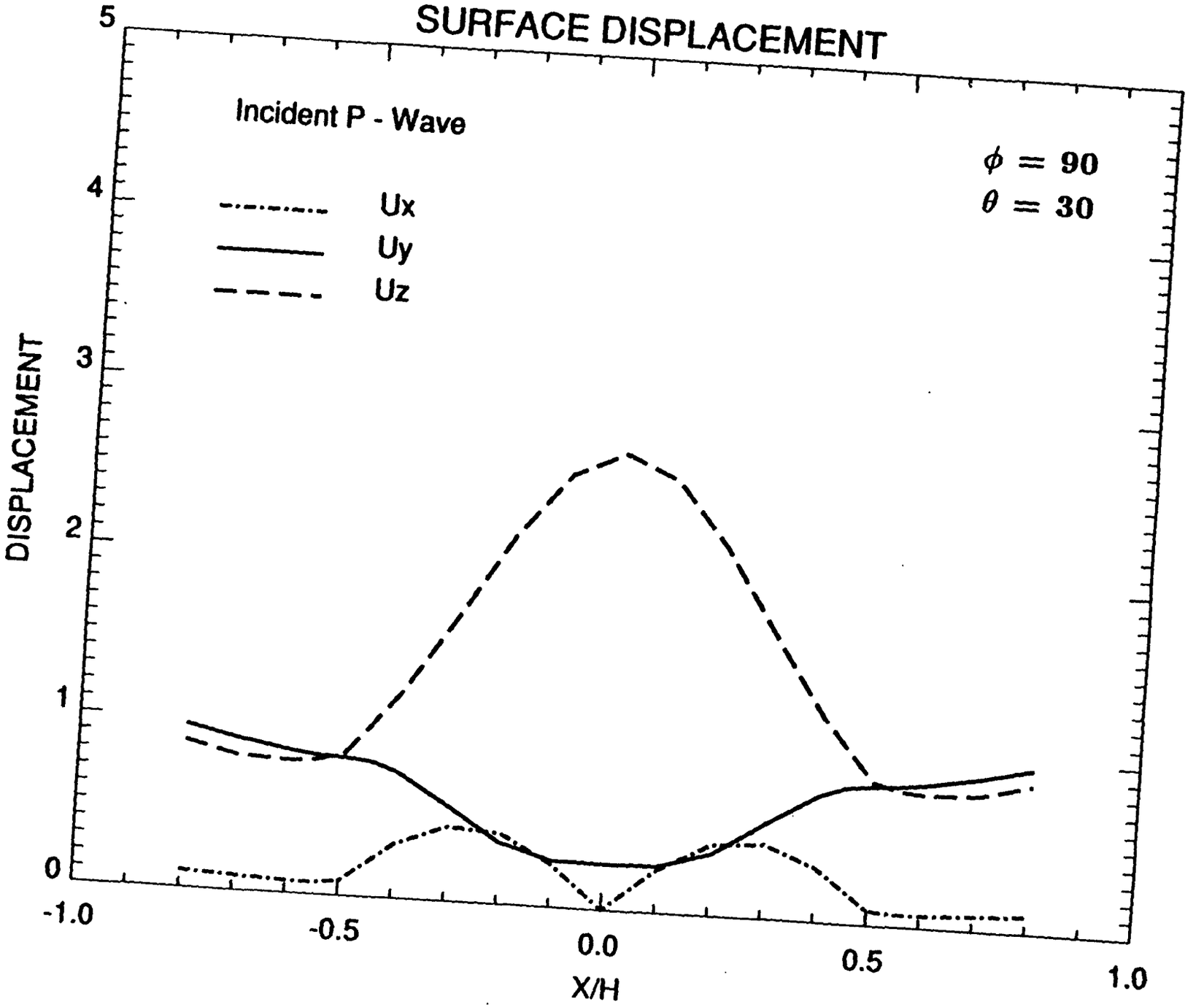
SURFACE DISPLACEMENT
Incident P - Wave
$\phi = 90$
$\theta = 30$
Ux
Uy
Uz
DISPLACEMENT
5
4
3
2
1
0
-1.0
-0.5
0.0
0.5
1.0
X/H

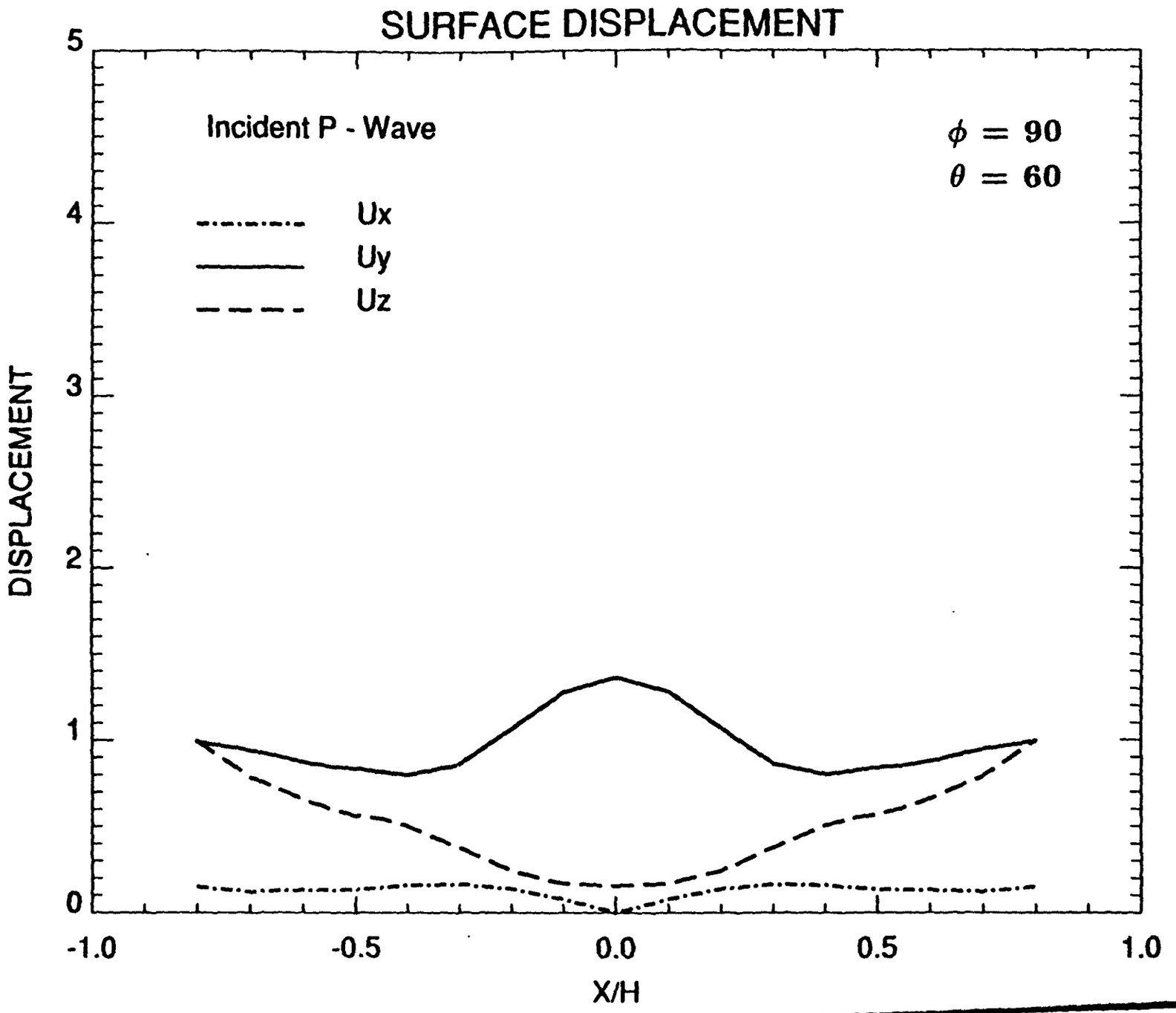
SURFACE DISPLACEMENT
Incident P - Wave
$\phi = 90$
$\theta = 60$
Ux
Uy
Uz
DISPLACEMENT
5
4
3
2
1
0
-1.0
-0.5
0.0
0.5
1.0
X/H

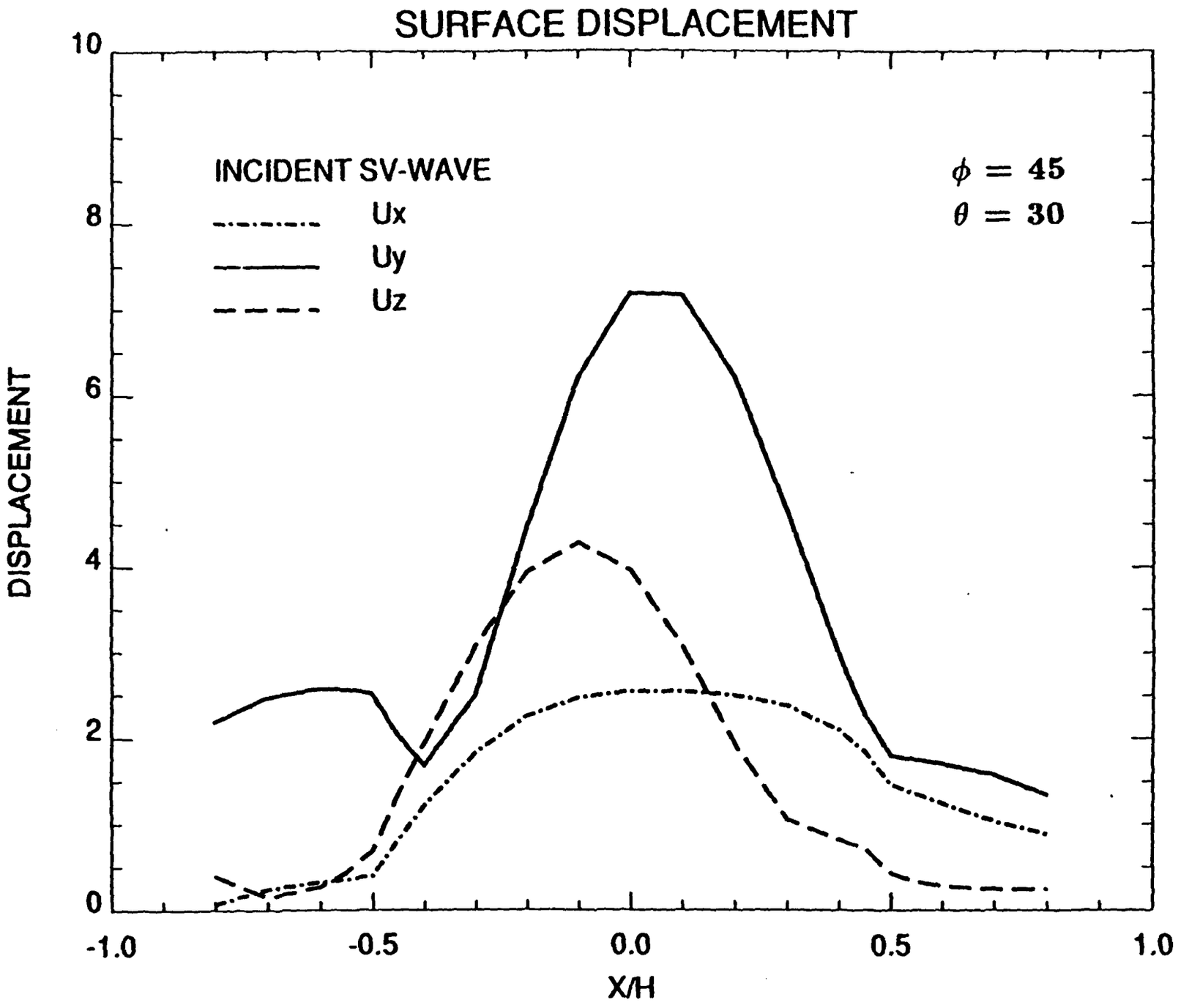
SURFACE DISPLACEMENT
INCIDENT SV-WAVE
Ux
Uy
Uz
$\phi = 45$
$\theta = 30$
DISPLACEMENT
10
8
6
4
2
0
-1.0
-0.5
0.0
0.5
1.0
X/H

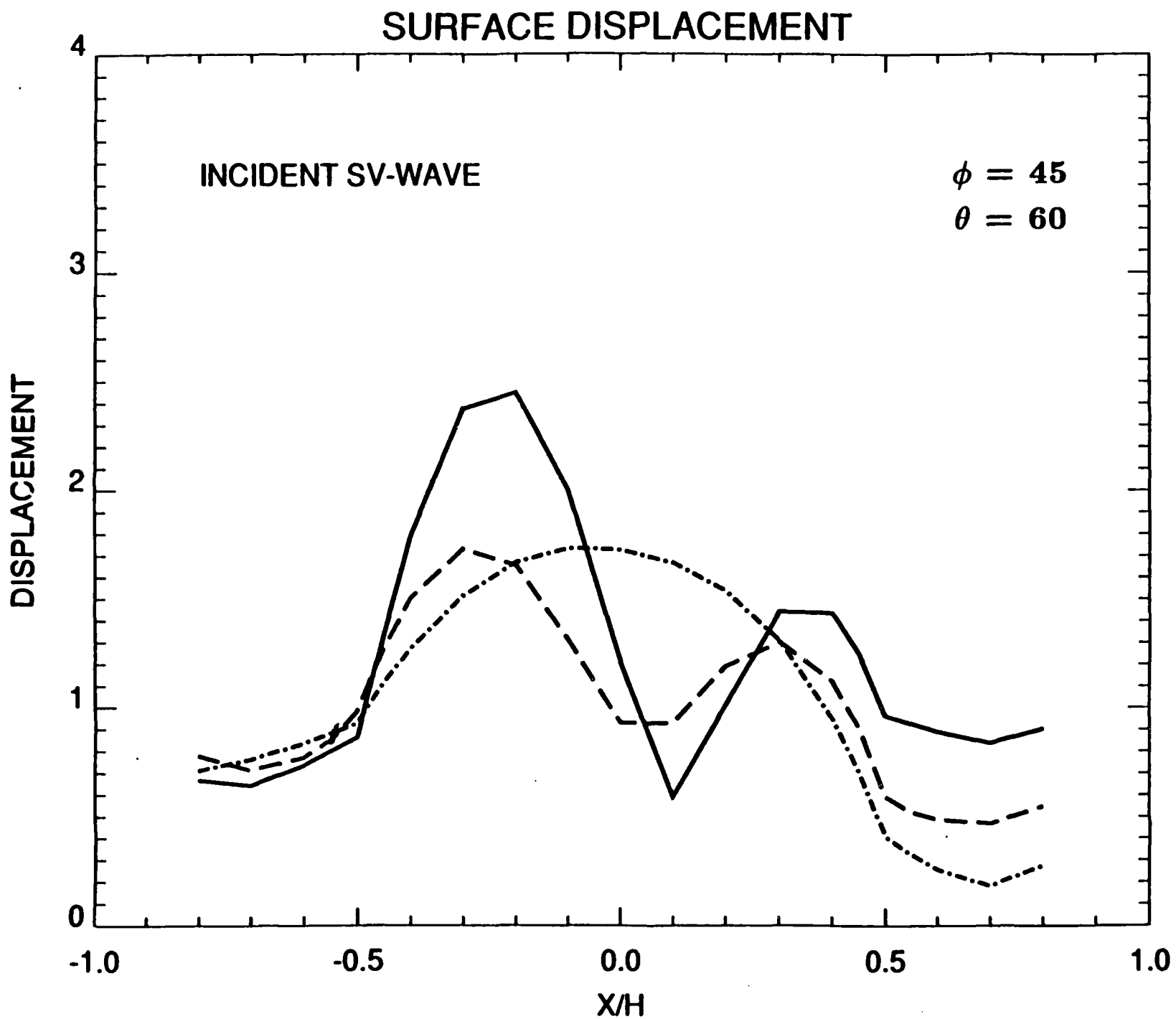
SURFACE DISPLACEMENT
INCIDENT SV-WAVE
$\phi = 45$
$\theta = 60$
DISPLACEMENT
X/H
4
3
2
1
0
-1.0
-0.5
0.0
0.5
1.0

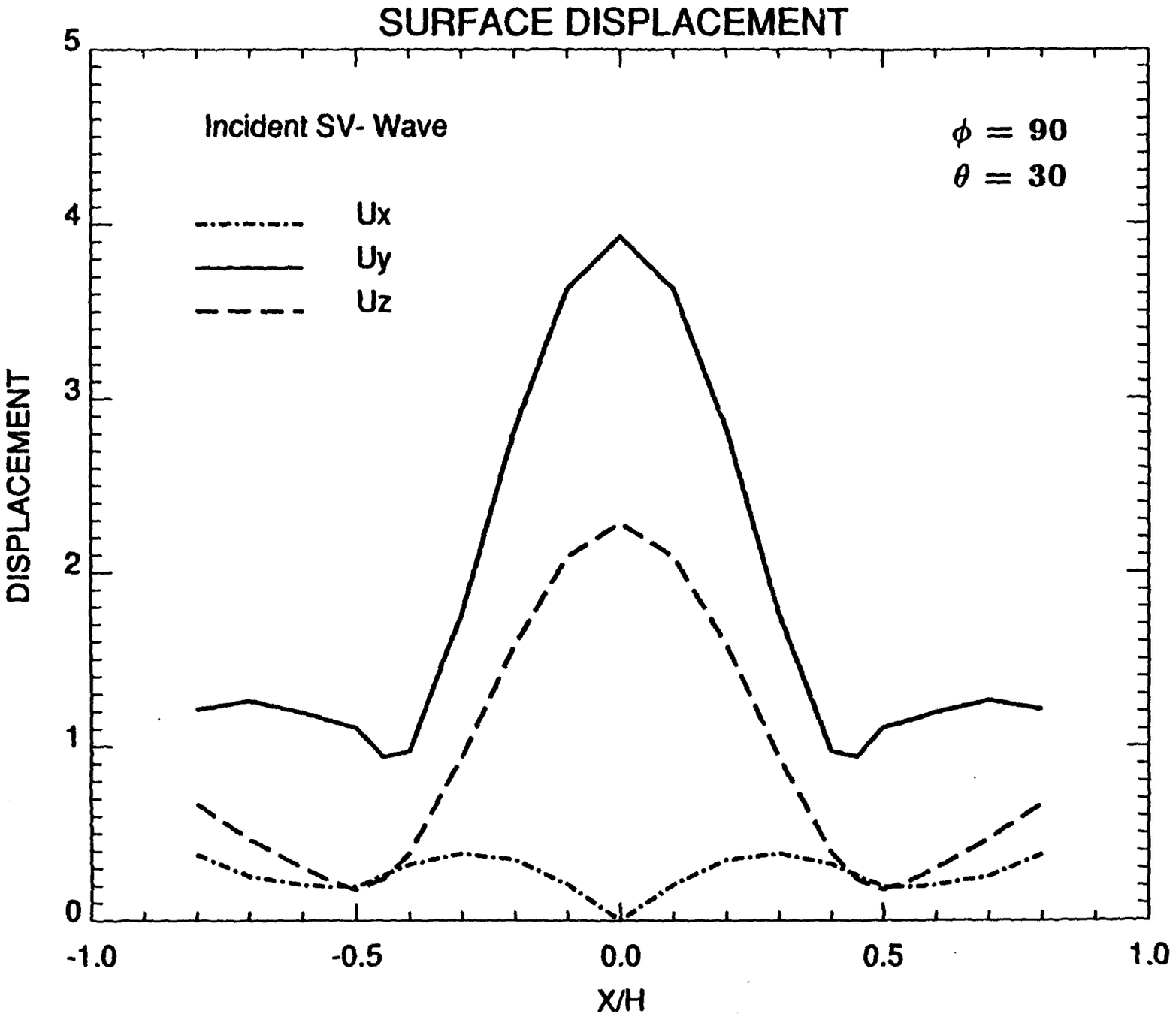
SURFACE DISPLACEMENT
Incident SV- Wave
$\phi = 90$
$\theta = 30$
Ux
Uy
Uz
DISPLACEMENT
X/H
5
4
3
2
1
0
-1.0
-0.5
0.0
0.5
1.0

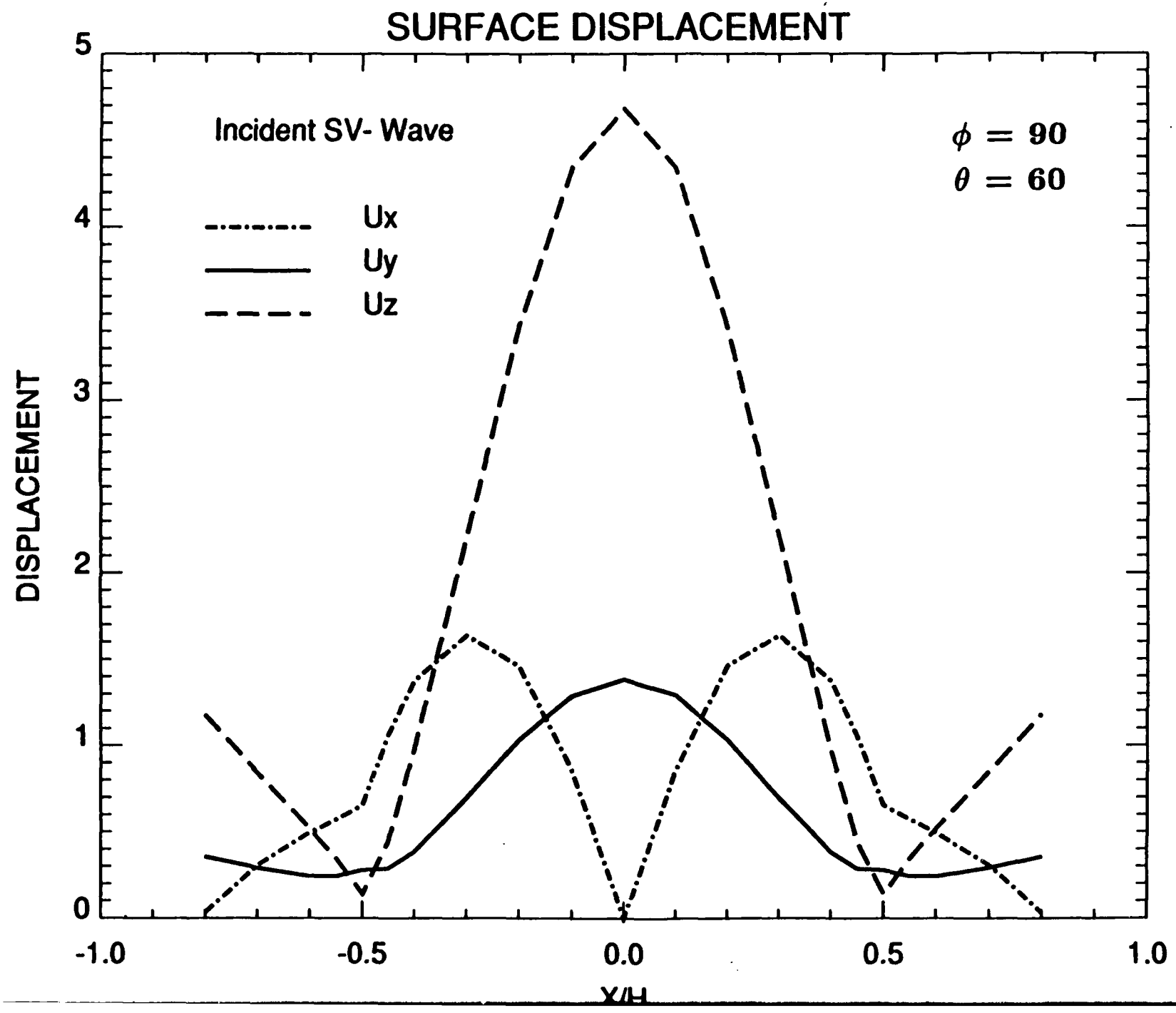
SURFACE DISPLACEMENT
Incident SV- Wave
$\phi = 90$
$\theta = 60$
Ux
Uy
Uz
DISPLACEMENT
5
4
3
2
1
0
-1.0
-0.5
0.0
0.5
1.0
X/H

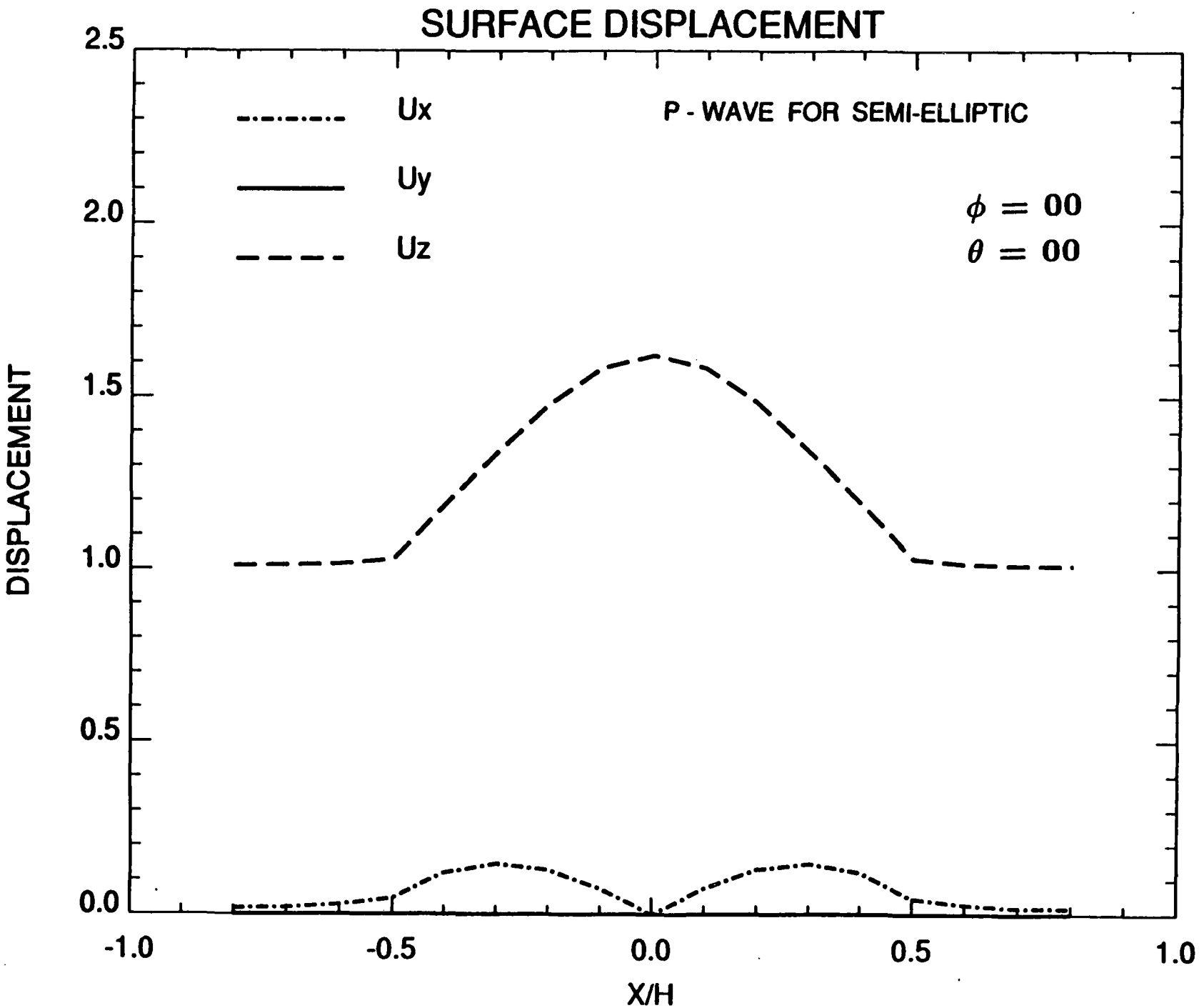
SURFACE DISPLACEMENT
P - WAVE FOR SEMI-ELLIPTIC
Ux
Uy
Uz
$\phi = 00$
$\theta = 00$
DISPLACEMENT
2.5
2.0
1.5
1.0
0.5
0.0
-1.0
-0.5
0.0
0.5
1.0
X/H

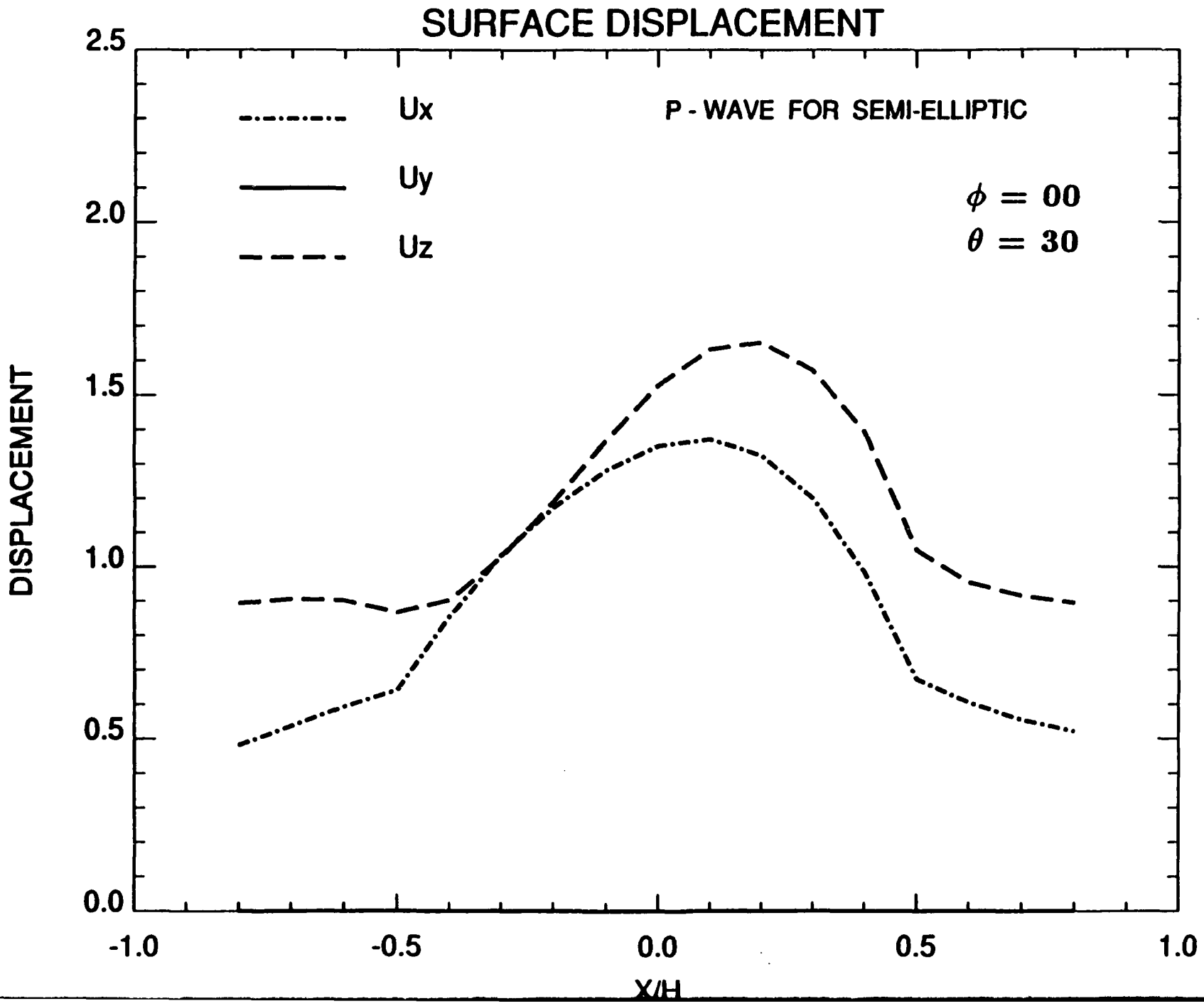
SURFACE DISPLACEMENT
P - WAVE FOR SEMI-ELLIPTIC
Ux
Uy
Uz
$\phi = 00$
$\theta = 30$
DISPLACEMENT
2.5
2.0
1.5
1.0
0.5
0.0
-1.0
-0.5
0.0
0.5
1.0
X/H

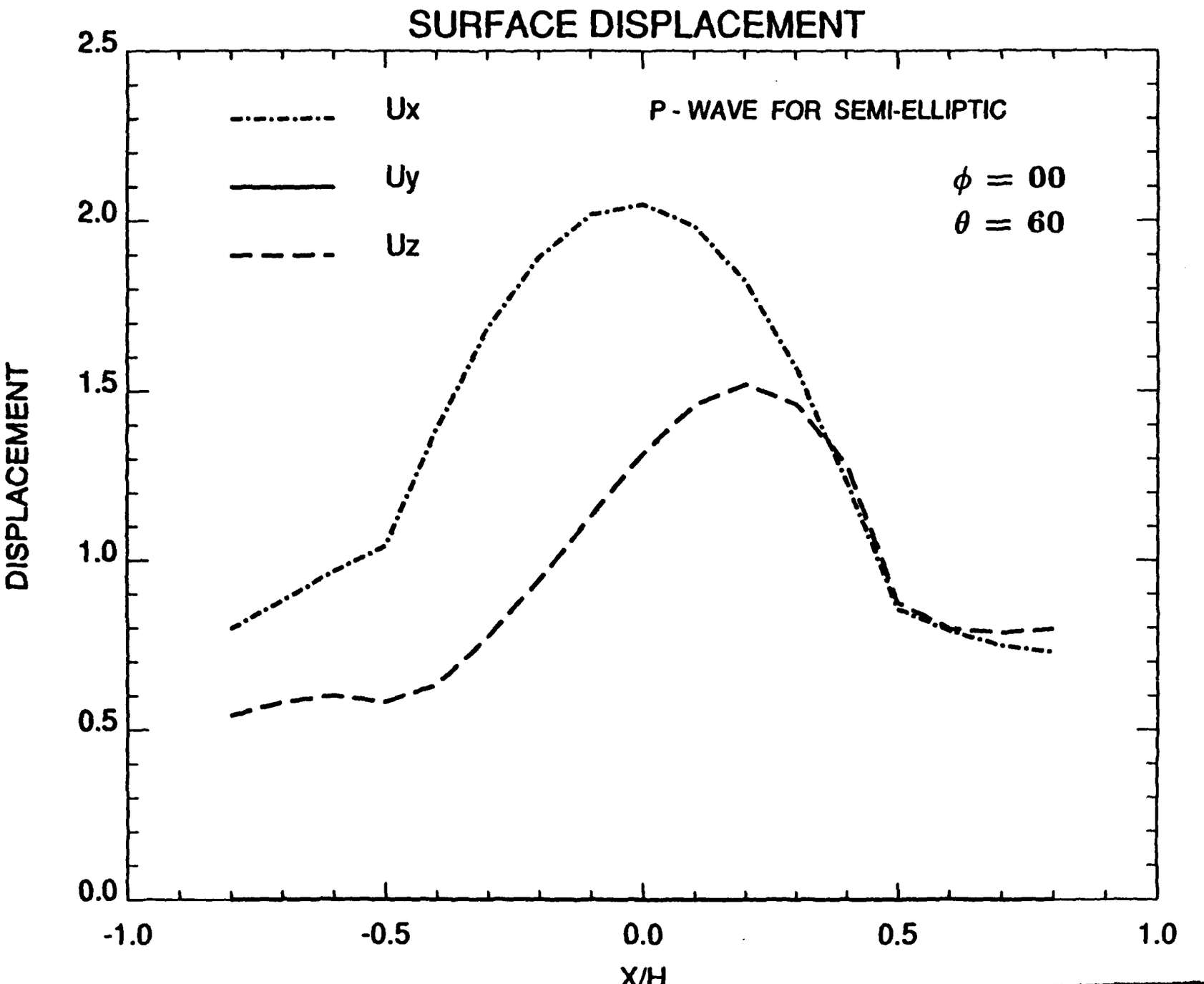
SURFACE DISPLACEMENT
Ux
Uy
Uz
P - WAVE FOR SEMI-ELLIPTIC
$\phi = 00$
$\theta = 60$
DISPLACEMENT
2.5
2.0
1.5
1.0
0.5
0.0
-1.0
-0.5
0.0
0.5
1.0
X/H

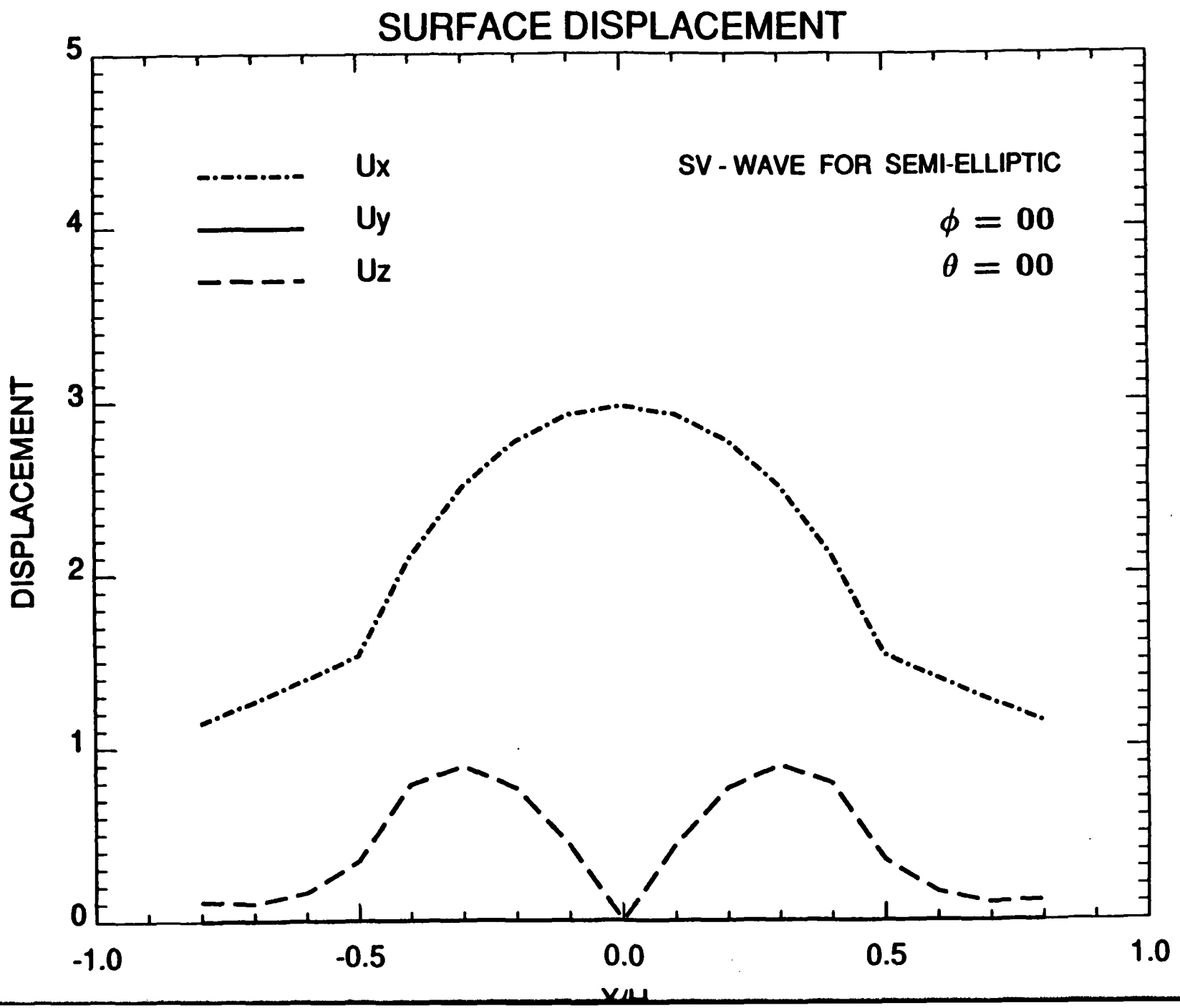
SURFACE DISPLACEMENT
Ux
Uy
Uz
SV - WAVE FOR SEMI-ELLIPTIC
$\phi = 00$
$\theta = 00$
DISPLACEMENT
5
4
3
2
1
0
-1.0
-0.5
0.0
0.5
1.0

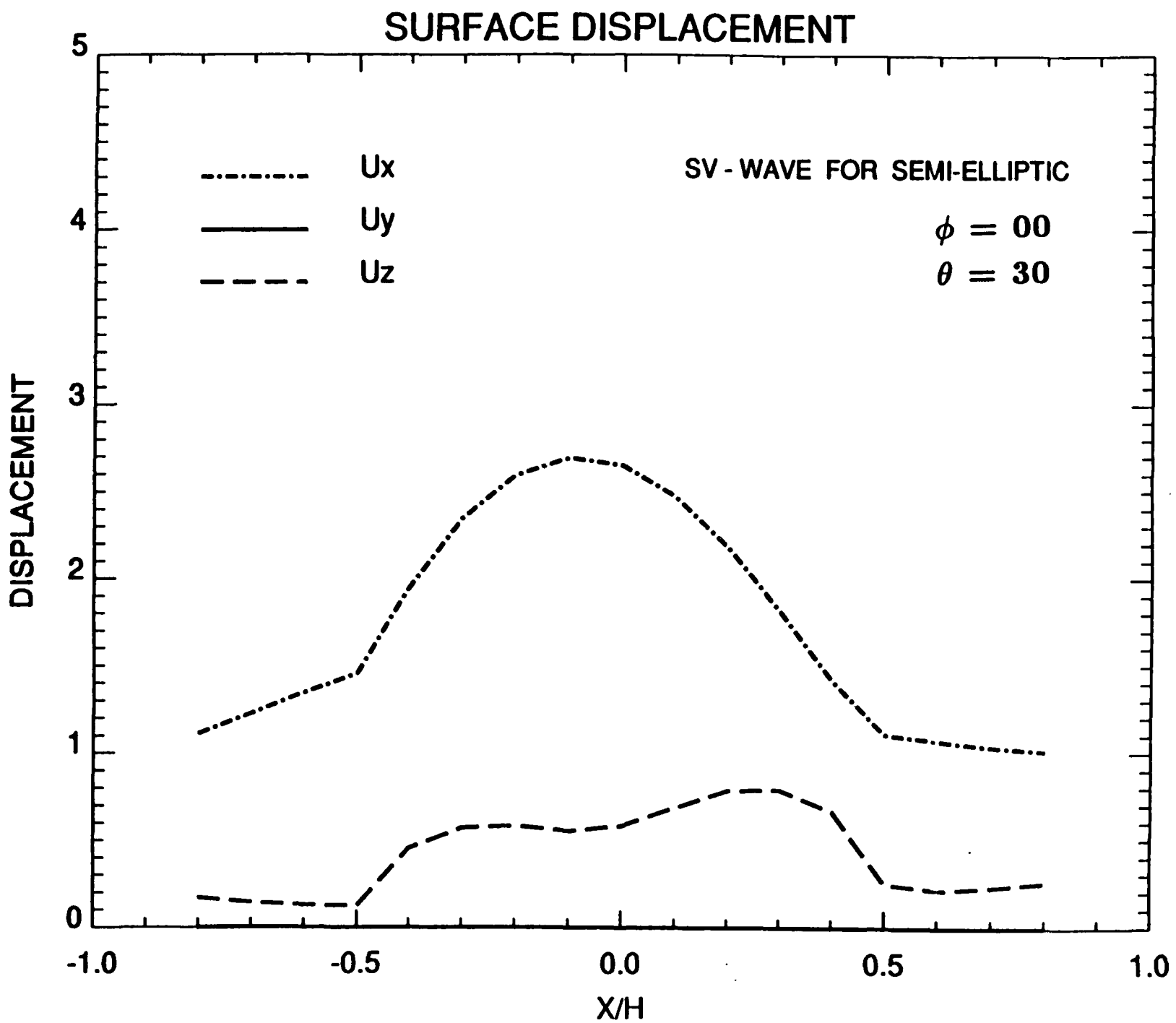
SURFACE DISPLACEMENT
Ux
Uy
Uz
SV - WAVE FOR SEMI-ELLIPTIC
$\phi = 00$
$\theta = 30$
DISPLACEMENT
0
1
2
3
4
5
-1.0
-0.5
0.0
0.5
1.0
X/H

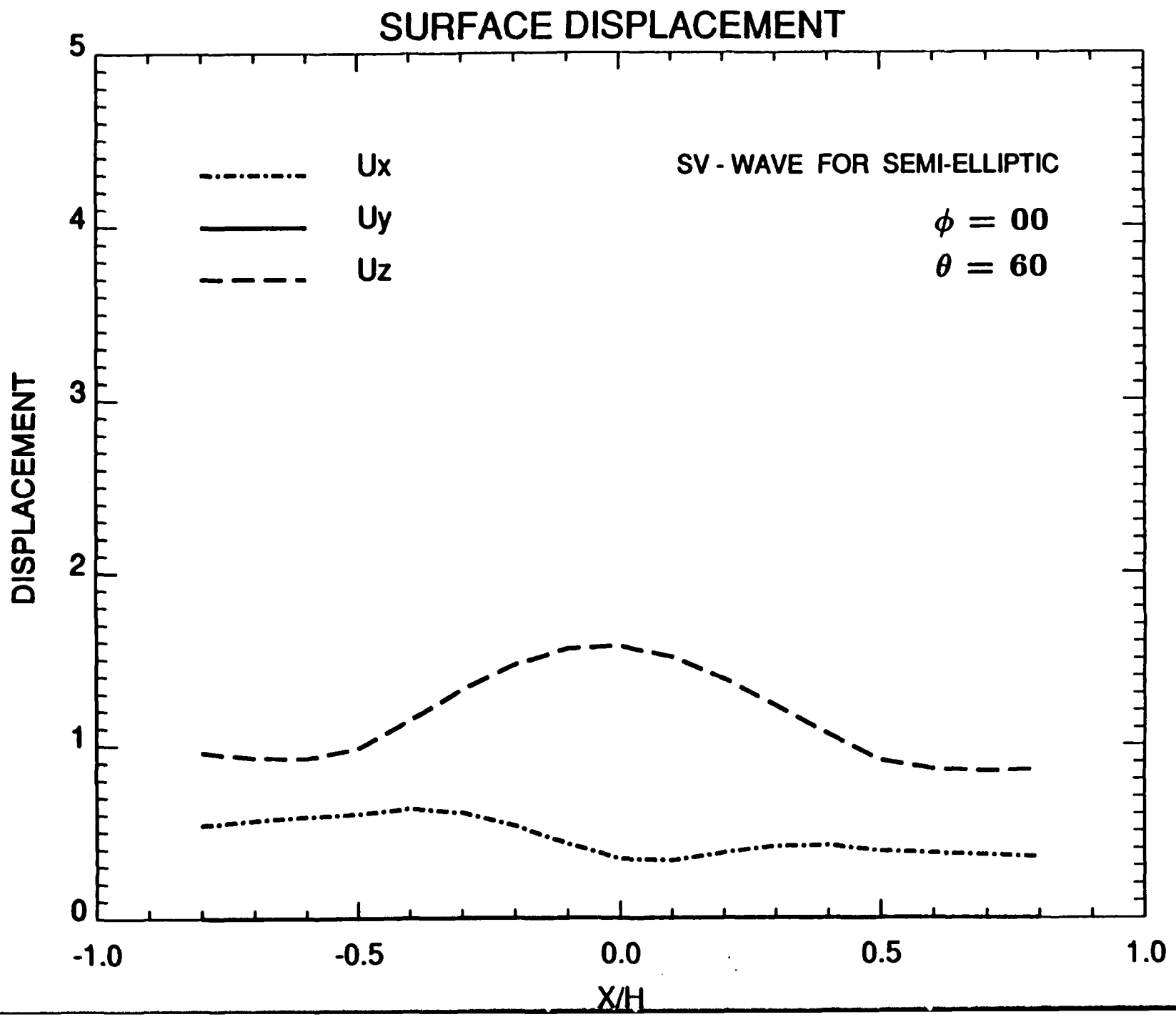
SURFACE DISPLACEMENT
Ux
Uy
Uz
SV - WAVE FOR SEMI-ELLIPTIC
$\phi = 00$
$\theta = 60$
DISPLACEMENT
5
4
3
2
1
0
-1.0
-0.5
0.0
0.5
1.0
X/H

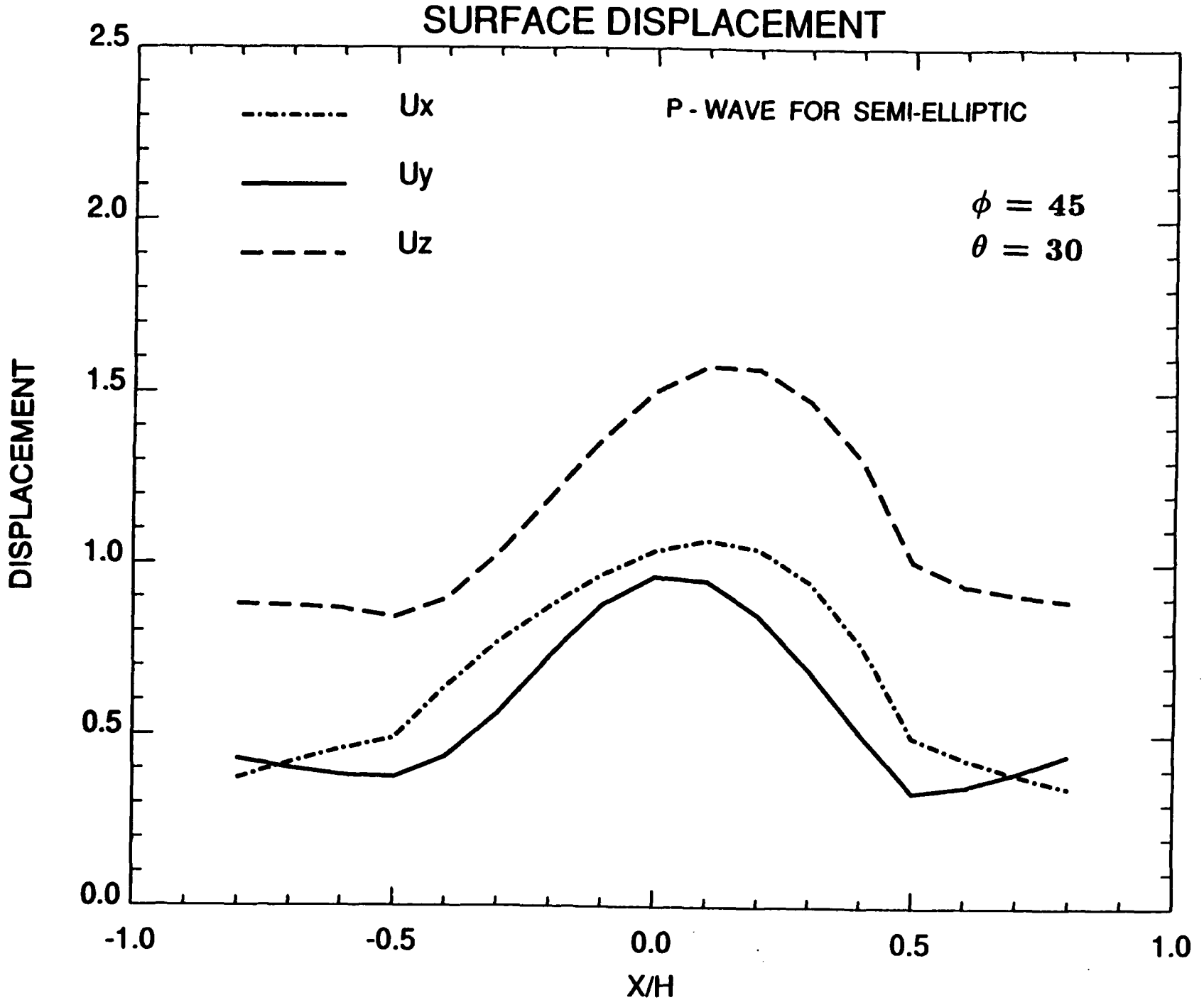
SURFACE DISPLACEMENT
P - WAVE FOR SEMI-ELLIPTIC
Ux
Uy
Uz
$\phi = 45$
$\theta = 30$
DISPLACEMENT
2.5
2.0
1.5
1.0
0.5
0.0
-1.0
-0.5
0.0
0.5
1.0
X/H

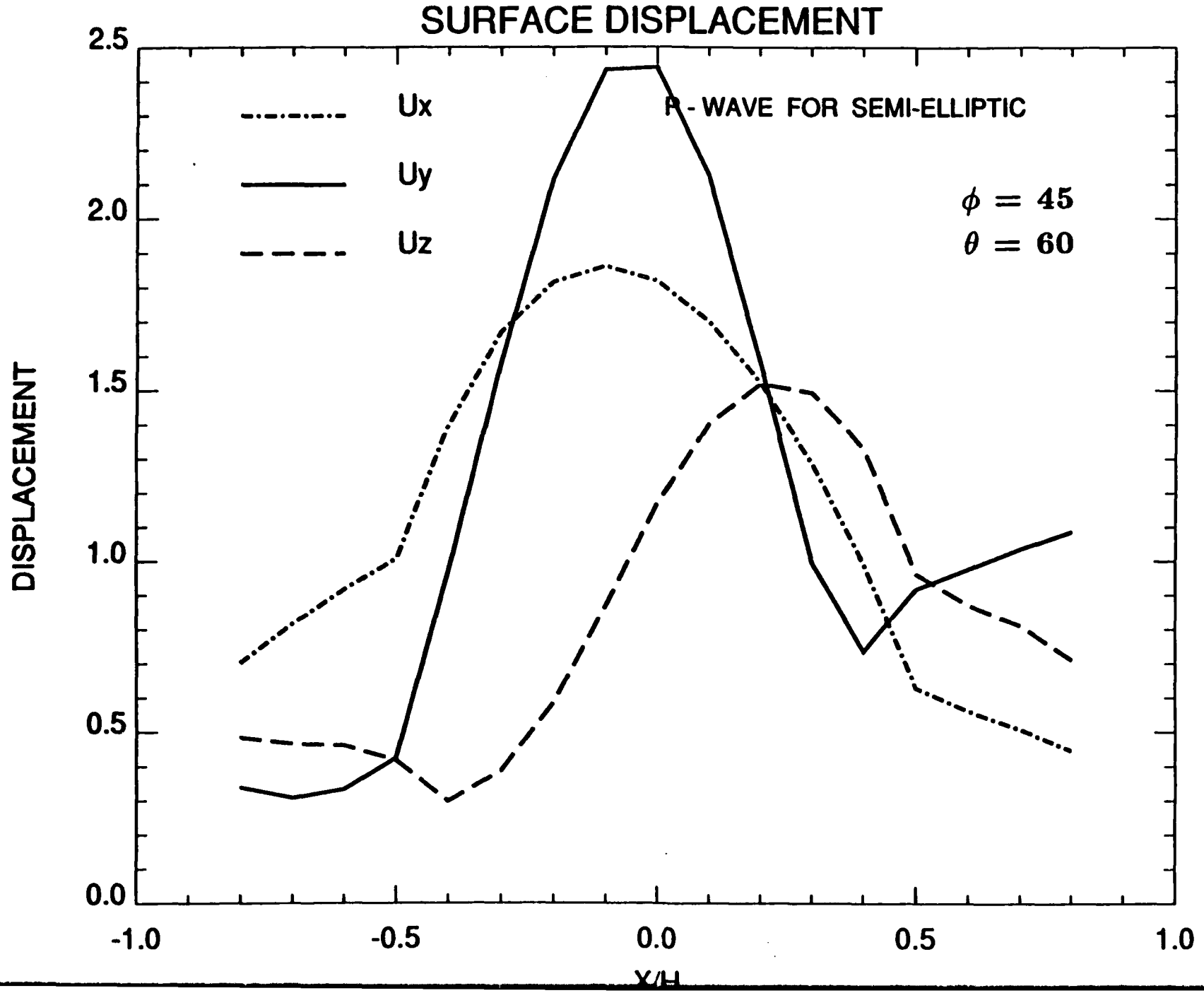
SURFACE DISPLACEMENT
Ux
Uy
Uz
P - WAVE FOR SEMI-ELLIPTIC
$\phi = 45$
$\theta = 60$
DISPLACEMENT
2.5
2.0
1.5
1.0
0.5
0.0
-1.0
-0.5
0.0
0.5
1.0
X/H

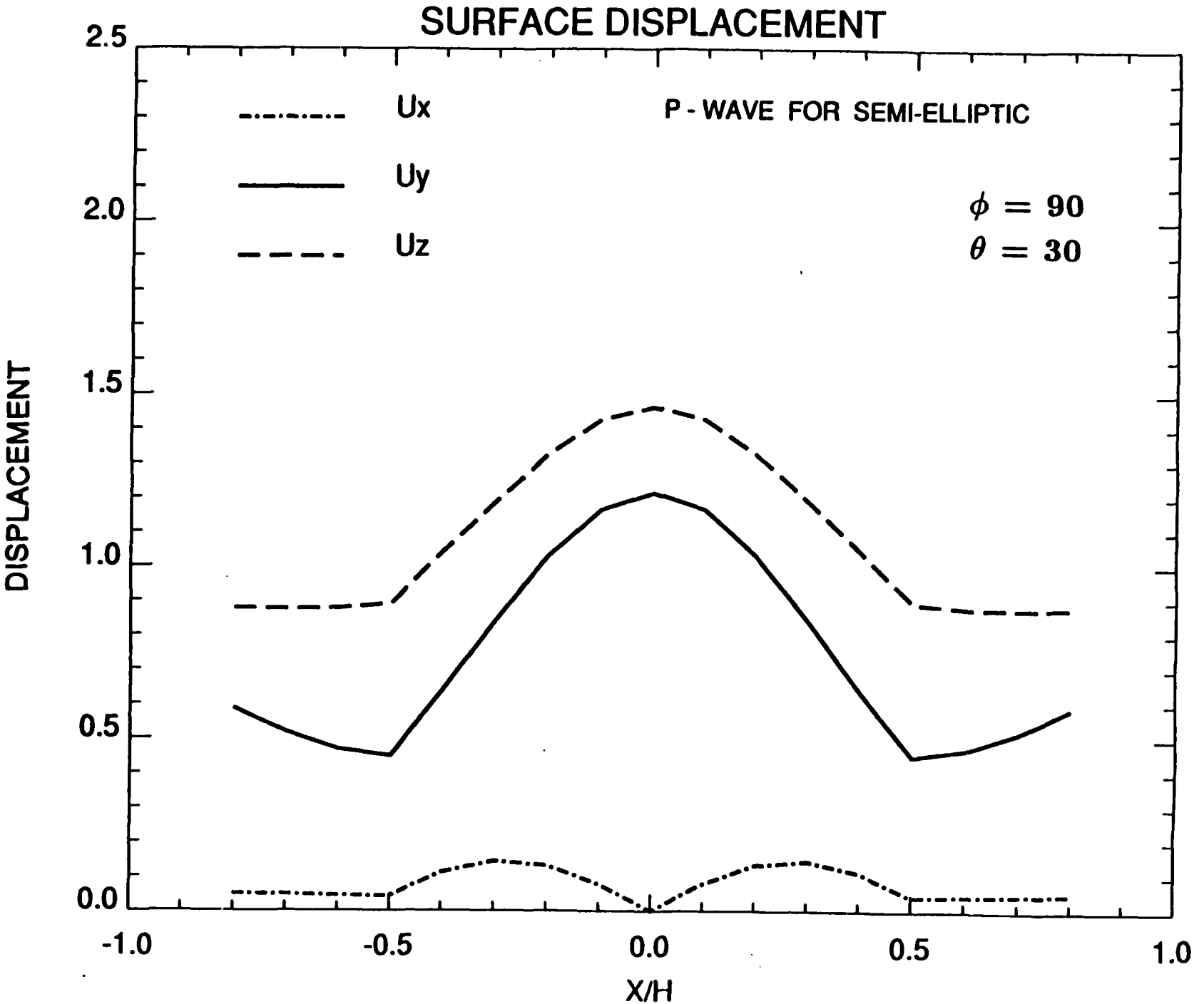
SURFACE DISPLACEMENT
P - WAVE FOR SEMI-ELLIPTIC
Ux
Uy
Uz
$\phi = 90$
$\theta = 30$
DISPLACEMENT
2.5
2.0
1.5
1.0
0.5
0.0
-1.0
-0.5
0.0
0.5
1.0
X/H

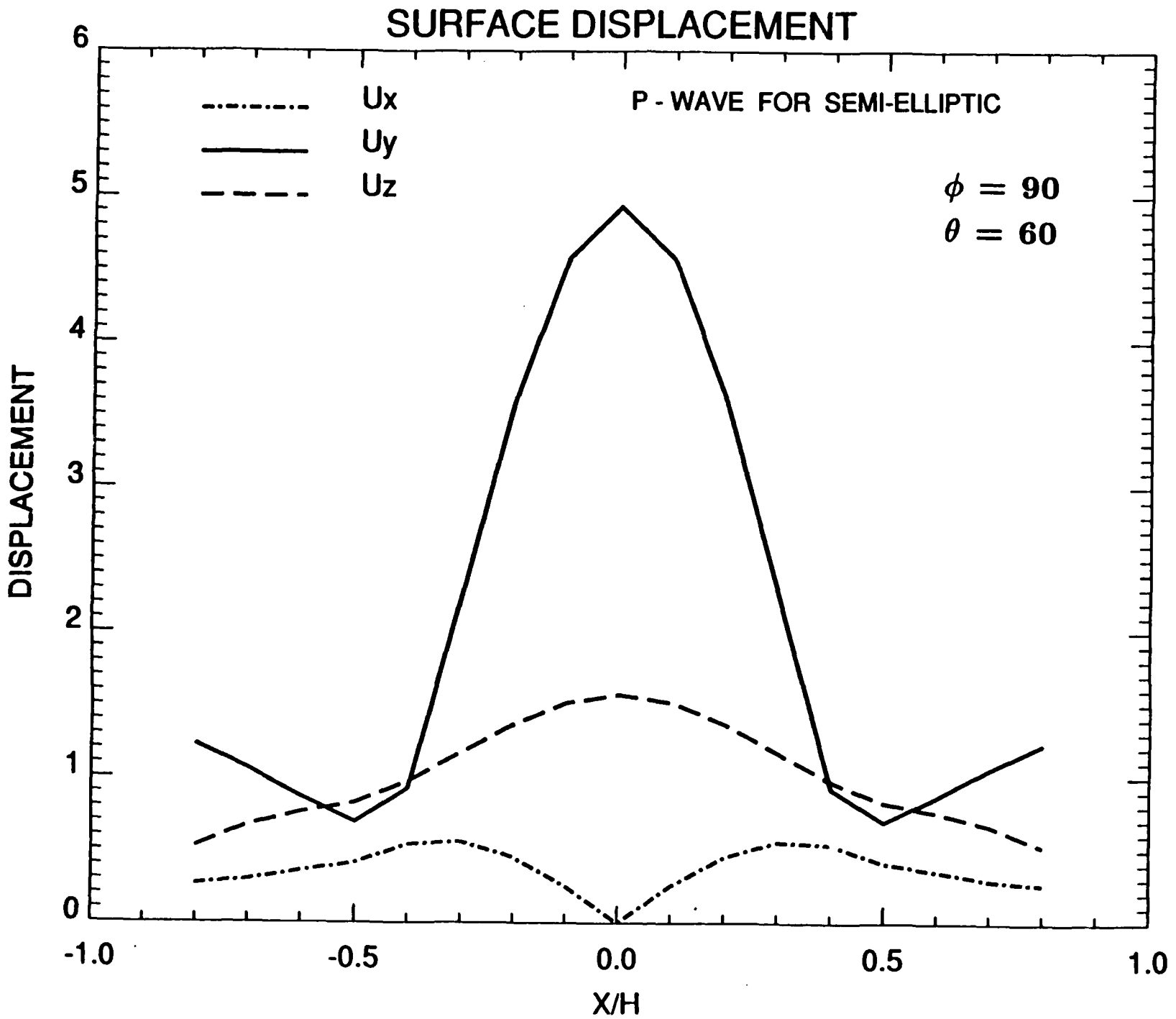
SURFACE DISPLACEMENT
P - WAVE FOR SEMI-ELLIPTIC
Ux
Uy
Uz
$\phi = 90$
$\theta = 60$
DISPLACEMENT
X/H
6
5
4
3
2
1
0
-1.0
-0.5
0.0
0.5
1.0

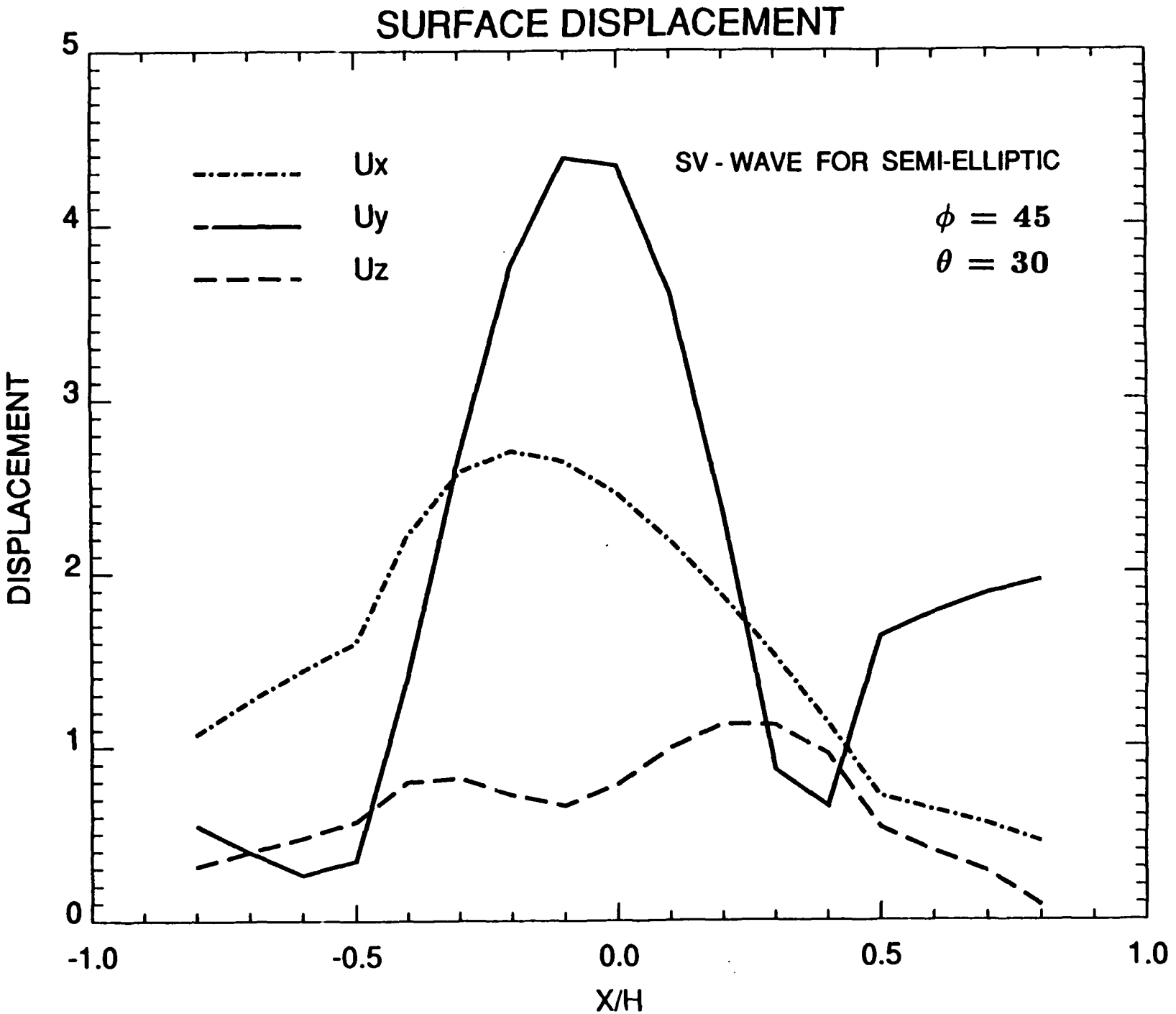
SURFACE DISPLACEMENT
SV - WAVE FOR SEMI-ELLIPTIC
$\phi = 45$
$\theta = 30$
Ux
Uy
Uz
DISPLACEMENT
X/H
5
4
3
2
1
0
-1.0
-0.5
0.0
0.5
1.0

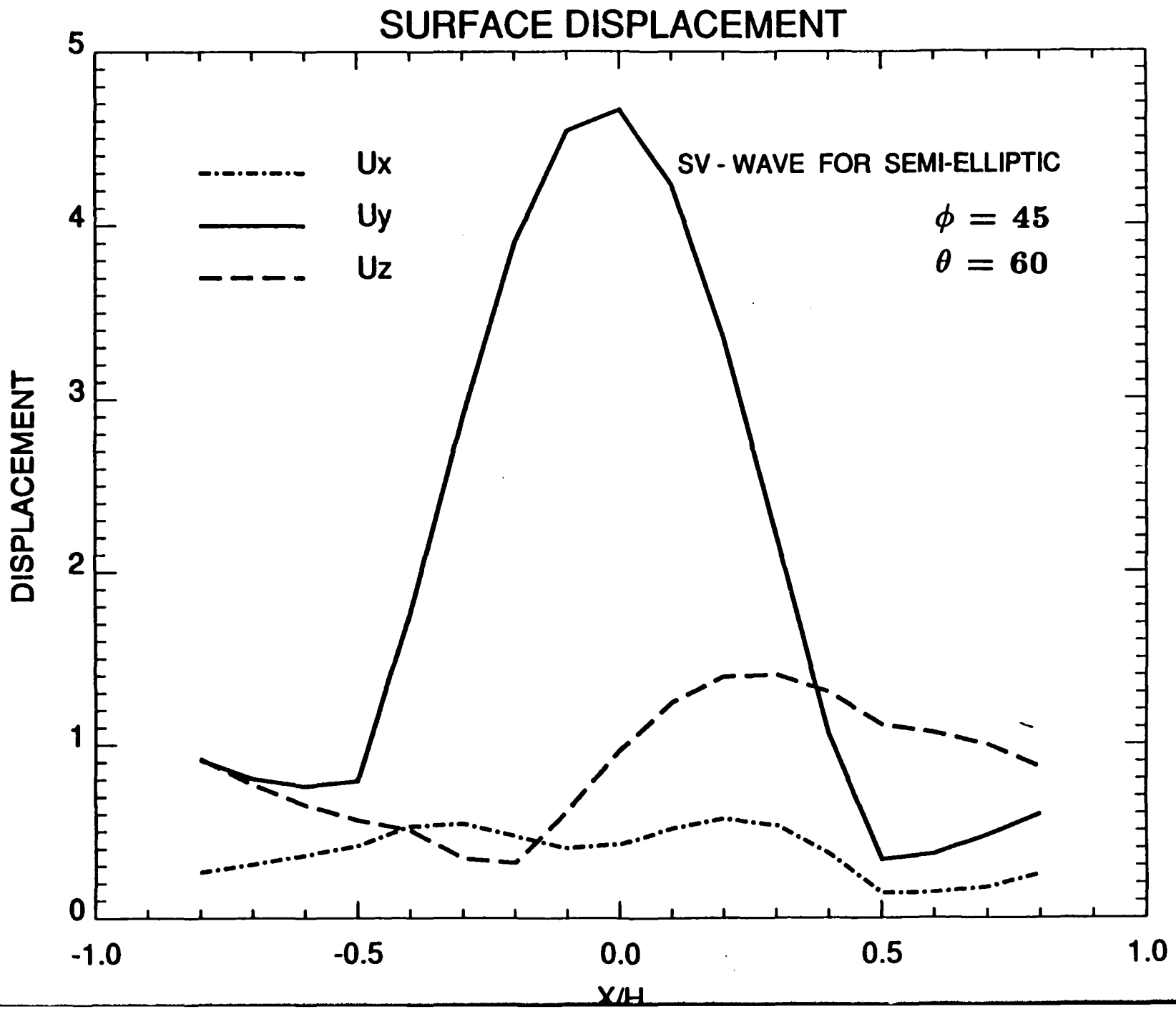
SURFACE DISPLACEMENT
Ux
Uy
Uz
SV - WAVE FOR SEMI-ELLIPTIC
$\phi = 45$
$\theta = 60$
DISPLACEMENT
5
4
3
2
1
0
-1.0
-0.5
0.0
0.5
1.0
X/H

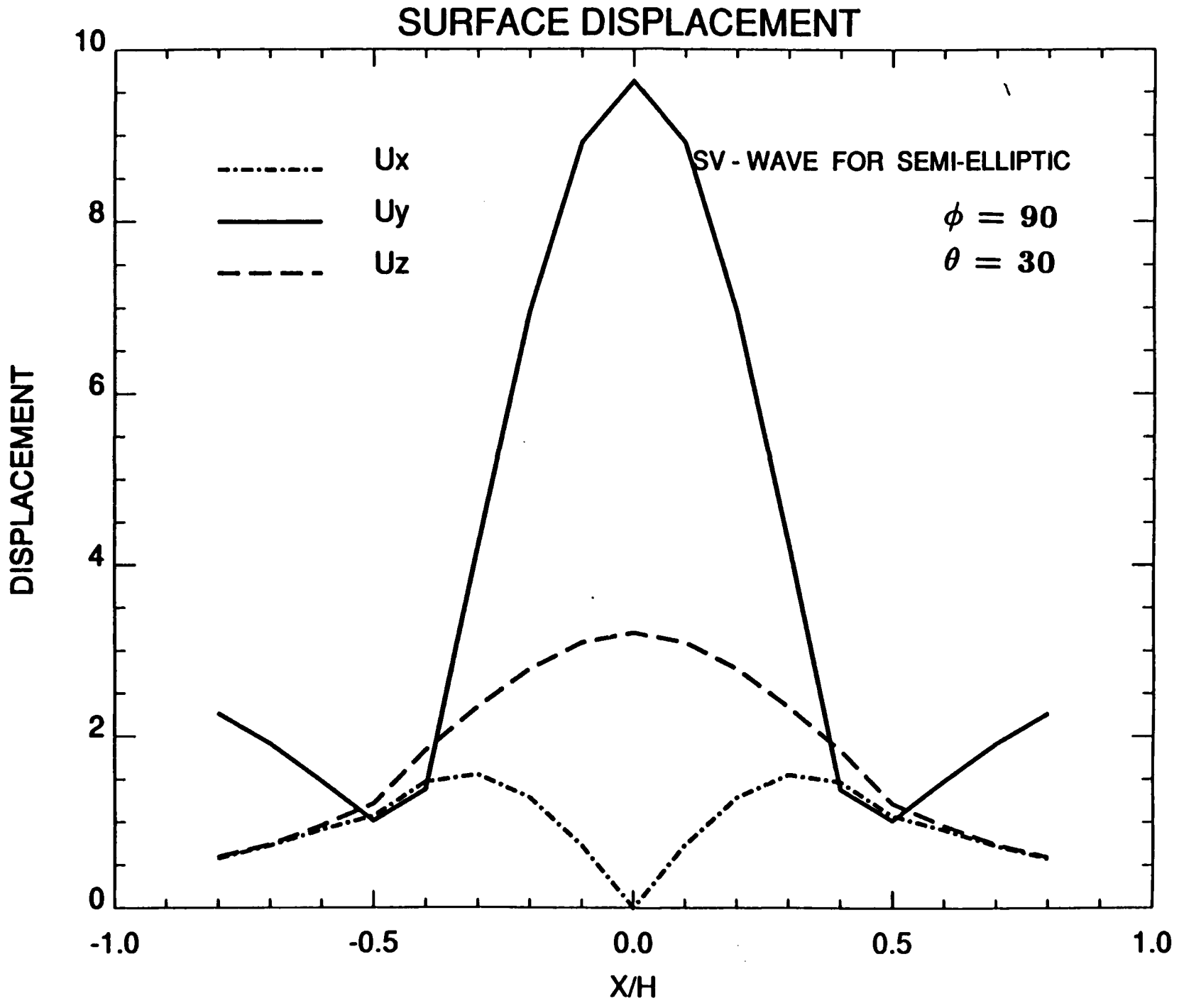
SURFACE DISPLACEMENT
Ux
Uy
Uz
SV - WAVE FOR SEMI-ELLIPTIC
$\phi = 90$
$\theta = 30$
DISPLACEMENT
10
8
6
4
2
0
-1.0
-0.5
0.0
0.5
1.0
X/H

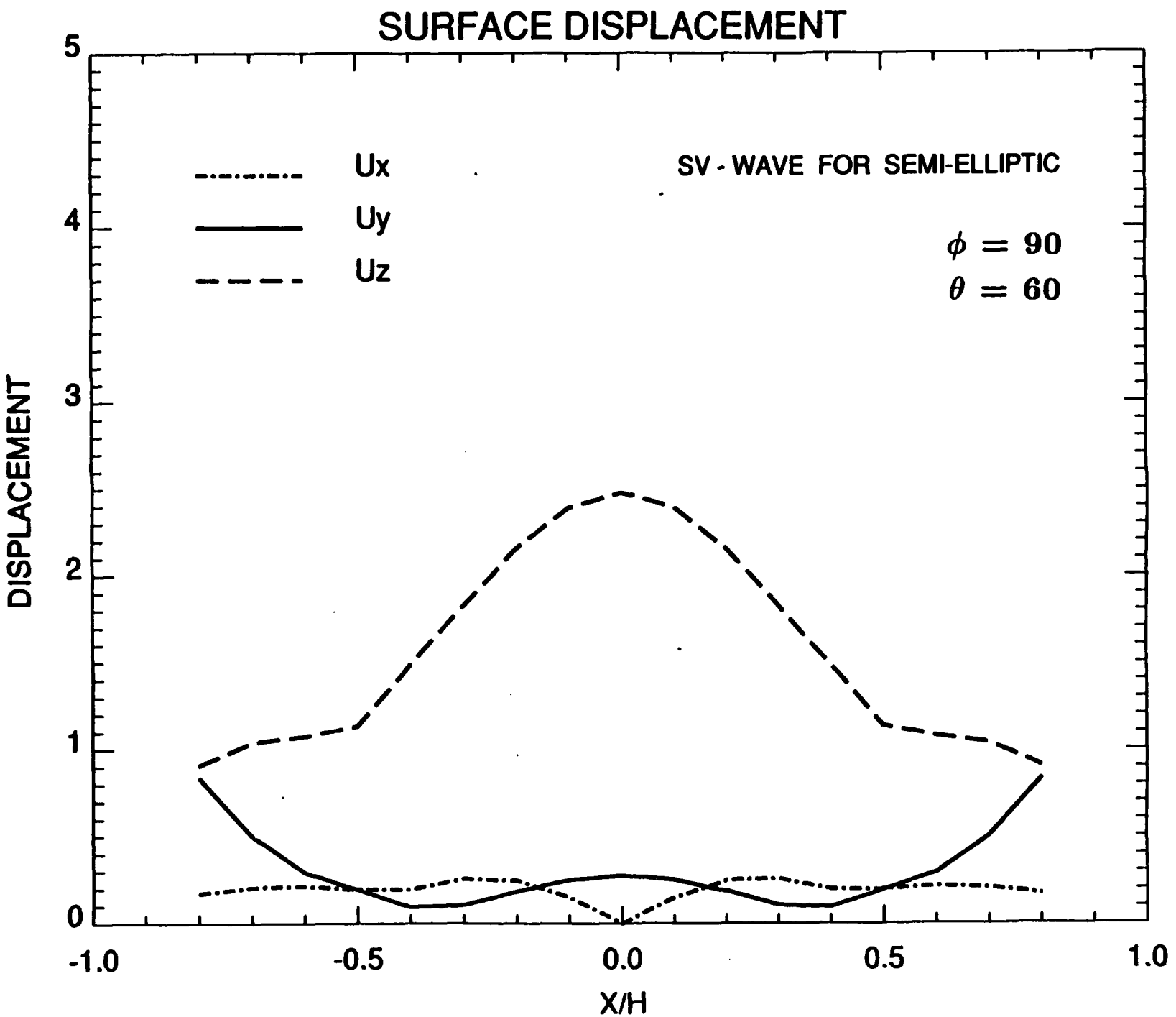
SURFACE DISPLACEMENT
Ux
Uy
Uz
SV - WAVE FOR SEMI-ELLIPTIC
$\phi = 90$
$\theta = 60$
DISPLACEMENT
5
4
3
2
1
0
-1.0
-0.5
0.0
0.5
1.0
X/H